American Mineralogist, Volume 91, pages 979–996, 2006

The origin of jadeitite-forming subduction-zone fluids: CL-guided SIMS oxygen-isotope and trace-element evidence

SORENA SORENSEN,[1,*] GEORGE E. HARLOW,[2] AND DOUGLAS RUMBLE III[3]

[1]Department of Mineral Sciences, National Museum of Natural History, Smithsonian Institution, Washington, D.C. 20560-0119, U.S.A.
[2]Department of Earth and Planetary Sciences, American Museum of Natural History, Central Park West at 79th St., New York, New York 10024, U.S.A.
[3]Geophysical Laboratory, Carnegie Institution of Washington, 5541 Broad Branch Road NW, Washington, D.C. 20015, U.S.A.

ABSTRACT

Jadeitite, a rare high *P/T* rock, is associated spatially with blueschist and/or eclogite terranes. Scanning electron microscope (SEM) and cathodoluminescence (CL) petrography of jadeitite samples from several major occurrences [in Burma (Myanmar), Guatemala, Japan, Kazakhstan, and the U.S.A.] show that grains were deposited from fluids. Jadeite grain compositions indicate these fluid compositions changed with time.

CL imagery guided the acquisition of oxygen-isotope and trace-element analyses with the ion microprobe. Jadeite grains in each rock grew in cycles that began with red- and/or blue-luminescent and ended with green-luminescent zones. The CL images were used to order the data into crystallization sequences. These data and electron-microprobe, major-element analyses document the association of green CL with increases in Ca, Mg, and Cr: (1) toward grain exteriors; (2) in fine-grained matrix around porphyroblasts; (3) in shear zones that cut grains; (4) in former open spaces now filled with jadeite; or (5) in veins. Abundances of many trace elements are greater in green-CL jadeitite compared with the red- or blue-CL zones. Some of these elements—in particular Li, Rb, Sr, Ti, Hf, Zr, Y, and REE—are unlikely to have been derived from serpentinite. Although crystal-chemical effects may explain some of the trace-element systematics (e.g., preferential incorporation of REE into Ca-richer jadeite), some kinetic control is suggested by sector-zoned, rhythmically zoned grains. The oxygen-isotope data suggest that jadeitite-depositing fluids either had multiple sources or evolved in composition along their flow paths (or both).

Keywords: Gems and gemstones, metamorphic petrology, analysis, chemical, major and minor elements, trace elements and REE, stable isotopes, petrography

INTRODUCTION

Rocks and minerals from subduction complexes and volcanic arcs provide direct evidence that subduction-zone fluids are complex, multicomponent entities that transfer components (e.g., LILE and LREE) from the variably altered slab (as well as from subducted sediments) to subarc mantle (e.g., Bebout and Barton 1993; Peacock 1993a, 1993b; Tatsumi and Eggins 1995, Bebout et al. 1996, 1999; Leeman 1996; Ryan et al. 1996; Spandler et al. 2003). Experimental studies suggest that, depending on *P-T* conditions, a variety of components are soluble in aqueous fluids under subduction-zone conditions (Manning 1998). Aqueous fluids can be sourced from dewatering and are also likely products of major types of subduction-related dehydration reactions in the slab and its subducted sediment carapace (Peacock 1990, 1991; Moran et al. 1992; Domanik et al. 1993; Bebout et al. 1999; Spandler et al. 2003). The geochemical action of fluids in subduction zones has been inferred from both the ultimate products of the system, volcanic arc rocks (Morris et al. 1990; Peacock 1991; Schmidt and Poli 1998; Class et al. 2000), and from proposed fluid effects upon the stable- and radiogenic-isotope compositions of variably metasomatized rocks of subduction complexes (e.g., Bebout and Barton 1989; Miller and Cartwright 2000; Putlitz et al. 2000; Frueh-Green et al. 2001; Miller et al. 2001, 2002; Catlos and Sorensen 2003; Zack et al. 2003; Elliott et al. 2004). This study documents new evidence for the oxygen-isotope and trace-element composition and evolution of low-*T* subduction-zone fluids: jadeitite.

Jadeitite—a rock that consists predominantly of near-end-member jadeite pyroxene ($NaAlSi_2O_6$)—is known primarily as a highly valued gem in some non-Western cultures, in particular, in China and southeast Asia (e.g., Hughes et al. 2000). Because jadeitite is used as a gem and high-value lapidary (carving and sculpture) material, it is actively mined where it occurs in reasonable abundance and quality. Like most gem materials, jadeitite is rare, and is found in regions that generally remain, as H.S. Washington (1906) pointed out, "difficult of access, and in which the geological conditions are little known." However, our studies document a connection between jadeitites and high *P/T* metamorphic terrains and/or rocks (e.g., Harlow 1994; Harlow and Sorensen 2001; Harlow et al. 2003; Sisson et al. 2004; Harlow and Sorensen 2005). Because jadeitite has long been interpreted to be a metasomatic replacement rock (e.g., Yoder 1950), it is a natural target for investigations of fluid-rock interactions in

* E-mail: sorensen@si.edu

subduction zones.

This paper aims to show that the petrogenesis of jadeitite is relevant to the study of the fluid-rock interactions in subduction zones. The deposition of jadeite grains, and the evolution of their compositions with time testify both to the devolatilization process that attends the blueschist-to-eclogite transition and the compositions of subduction-zone fluids (e.g., Manning 1998, 2004), and to how fluids transport LILE, LREE, and HFSE through bodies of serpentinizing peridotite at depth in subduction zones. Jadeitite shows cathodoluminescence (CL) in blue, green, and red wavelengths, a property that has been exploited by gemologists for material identification and authentication (Ponalho 1986, 1999, 2000, 2002). The technique also documents the growth history of grains within specimens (Sorensen and Harlow 1998; Shi et al. 2000). The CL zoning of jadeitite is seemingly unique to each block, but with a suggestion of cycles of crystallization, as described below. To interpret the details of jadeite growth in the context of crystal-chemistry or geochemistry, the grain-growth histories seen in CL are combined with small-volume mineral analyses.

The geology of jadeitite

Jadeitite is found in only eight well-documented, primary, hard-rock occurrences: (1) Tawmaw Region of the Jade Mines District, Burma (Myanmar); (2) central Motagua Valley, Guatemala; (3) Omi-gawa and Kotaki-gawa drainages, Japan; (4) Oeyama ophiolite, Japan; (5) Ketchpel River, Polar Urals, Russia; (6) Itmurundy area, Kazakhstan; (7) Yenisey River region, Khakassia (West Sayan, Russia); and (8) New Idria, California. Other jadeitite deposits in Burma, Japan, and Kazakhstan are either of secondary origin (i.e., conglomerate-sourced) or poorly documented. A proposed source for jadeitite in Costa Rica, postulated to exist because of archeometric statistical analyses of Precolumbian jadeitite artifacts (Bishop et al. 1991, 1993), is geologically improbable (Harlow 1993). A site in Oaxaca, Mexico has been postulated on the basis of the distribution of Precolumbian jadeitite artifacts and the presence of serpentinite- and eclogite-bearing units in the Oaxaca region (e.g., Foshag 1957; Harlow 1993). However, no primary jadeitite source has been located there as of this writing.

Jadeitite localities show several common features. First, in-situ massive jadeitite is found as isolated bodies within serpentinite-matrix mélanges. The jadeitite bodies are described as veins, dikes, or rounded masses in a matrix of serpentinite (e.g., Harlow and Sorensen 2005). Some of these bodies are separated from their serpentinite host rocks by selvages of sodic and sodic-calcic amphibole (Shi et al. 2003) rock. In other cases, the same body of serpentinite-matrix mélange that contains jadeitite also hosts eclogite, garnet amphibolite, or blueschist, commonly in apparent close proximity to jadeitite bodies. Jadeitite, eclogite, garnet amphibolite, and blueschist are more resistant to weathering and erosion than are serpentinites. Rounded boulders of the former rock types are commonly found together in apparent lag deposits on the latter. In the most famous locality for massive jadeitite at Tawmaw, Burma, a now completely mined out jadeitite body of approximately 100 by 20 meters was interpreted in early scientific reports to have been an albite-granite dike that had been transformed metasomatically to jade (e.g., Chhibber 1934). In contrast, Harlow (1994) showed that margins of and veins in jadeitite bodies may consist of albitite, which may appear to have "granitic texture," but which is, in fact, a late-stage alteration product of jadeitite. Perhaps because albitite is so commonly associated with jadeitite, essentially all early workers and many active ones interpreted jadeitite to be derived from the metasomatism of granite or other felsic protoliths (Chhibber 1934; Chihara 1971; Dobretsov 1984).

Samples

Samples of jadeitite were obtained from the mineral collections of the National and American Museums of Natural History and from the Fersman Mineral Museum, Moscow (Table 1). In hand sample or thin section chip, the specimens range through diverse hues, from white with bright-green stringers, through creamy green and light straw, to pale pink (Table 1). This study collection consists predominantly of museum specimens, and some are undoubtedly from secondary (i.e., conglomerates or unconsolidated alluvial deposits; Hughes et al. 2000). Sample CJ-01 was collected by us and our colleagues in 2000 from a river that drains a conglomeratic (secondary) jadeitite deposit in Nansibon, Burma. Some of the specimens contain stringers that are vivid emerald green in color, but none was of translucent "imperial jade" material (Cr-rich jadeite does not luminesce).

Analytical methods

Polished thin sections were made for each sample. These were first examined with the petrographic microscope to verify that the sample consisted primarily of jadeite. Each thin section was examined and photographed for CL and then analyzed, first with the electron microprobe, and subsequently with the ion microprobe. In the following sections, all brand names are identified without the endorsement of either the Smithsonian Institution or the American Museum of Natural History.

Cathodoluminescence petrography

Between 1997 and 2002, some specimens were observed and photographed with an Olympus microscope camera, using Kodak Gold ASA200 film, mounted on a microscope attached to a Premier American Technologies luminoscope model ELM-3, in the Department of Mineral Sciences, National Museum of Natural History, Smithsonian Institution. Operating conditions were 20 kV and 0.5 mA. The film was developed and printed with Kodak film processing at a local business. From 2002 onward, images were collected using digital photography with an Olympus Opelco MagnaFire Model S99806 camera system, with associated software. Digital imaging with this system entails capturing three digital grayscale images with a 1300×1030 pixel monochrome CCD through a rotating R-B-G color filter wheel, then combining these R-B-G images with proprietary software. The CL figures (2 and 8) show both emulsion images scanned into Adobe Photoshop and digital images. Scanned emulsion images were corrected using "brightness" and "levels" corrections to visually reproduce the colors of the original photographs. The digital images were corrected by "sharpening" and "auto-levels," tools, which appear to reproduce best the colors actually seen in the glass window of the sample chamber.

Electron probe microanalysis

Specimens were analyzed using line scans on the JEOL JXA-8900R electron microprobe in the Smithsonian's Department of Mineral Sciences, using the mineral standards of Jarosewich et al. (1980), an accelerating voltage of 15 kV, and a probe current of 2×10^{-8} A. The counting time for each analysis point was 20 s on each element. Results are reported in Table 2. The CL images were one basis for navigation, in concert with transmitted and reflected light photographs.

In many cases, electron-beam damage to a grain during analysis changed the CL properties of that spot, and "post-microprobe" CL-imaging revealed linear tracks of ~2 to 3 μm diameter spots spaced 15 to 20 μm apart, the distance ranges specified for line analyses. Such samples could be indexed retrospectively to ascertain which CL color zone had been analyzed on a scale of tens of micrometers. For unknown

TABLE 1. Sample provenance and macroscopic features

Sample	Origin	Deposit	Country	Color
112538	Smithsonian	Motagua	Guatemala	Creamy Green
112552-1	Smithsonian	Kotaki	Japan	White with Bright Green Stringers
J-33-D	Smithsonian	New Idria, CA	USA	Light Straw
CJ-01	Smithsonian	Nansibon	Burma	Chalk White
BUR-07	Fersman Museum	Presumed Jade Tract	Burma	Pale Pink
102029	AMNH	Itmurundy	Kazakhstan	White with Bright Green Stringers
104276	AMNH	Itmurundy	Kazakhstan	White with Bright Green Stringers

reasons, not every sample showed easily distinguishable lines of spots, and parts of some lines were less distinct than others. In the former case, color-indexed data are lacking; in the latter, interpolation with a calibrated straight edge allowed lines of 10s to 100s of spots to be CL-color indexed.

Secondary ion mass spectrometry for trace-element analysis

Samples were analyzed with the Cameca 6F ion microprobe at the Department of Terrestrial Magnetism, Carnegie Institution of Washington. NIST glass standards were used for calibration and to monitor the performance of the instrument. No time-dependent drift corrections were made to the data set. Indeed, trace-element values for adjacent target sites in two samples (93803—not reported in this paper—and 112538) changed little between two successive years of analysis (Table 3).

Secondary ion mass spectrometry for oxygen-isotope analysis

Samples were analyzed with the Cameca 6F ion microprobe at the Department of Terrestrial Magnetism, Carnegie Institution of Washington. Three standards were used: jadeite, jadeite glass, and albite glass. All of these were analyzed and discussed by Eiler et al. (1997), and are useful monitors of instrument performance. Unlike the trace-element data, the raw oxygen-isotope data for the jadeite standard appeared to be strongly affected by instrumental drift over 5 days of analysis (Fig. 1). The changing apparent values for the jadeitite standard were roughly linear, with a small but statistically defensible decrease with time; the albite standard, which was only run three times, showed less evidence for drift (Fig. 1). The oxygen-isotope values of unknown samples were corrected to "no-drift" values for the standard, as defined by the dotted (jadeite) and dashed (albite) lines in Figure 1.

To evaluate whether the corrected ion microprobe values were similar to those obtained with methods that have intrinsically greater analytical precision, three samples of jadeite were handpicked from a subsample of the Eiler et al. (1997) material, as well as samples 112552-1 and J-33-D, and analyzed by the third author in the laser fluorination oxygen-isotope laboratory at the Geophysical Laboratory, Carnegie Institute of Washington. Garnet standard UWG-2 (Valley et al. 1995) also was analyzed. The garnet yielded $\delta^{18}O$ values of +5.86 and 5.74‰, in good agreement with the recommended value of $\delta^{18}O = +5.8$‰ relative to SMOW. The results for jadeite are scattered, in part by the difficulties caused by the response of this mineral to laser fluorination. The jadeite mineral standard for the ion microprobe that was described by Eiler et al. (1997) yielded $\delta^{18}O$ values of +8.51 and 9.39‰ for grains from a hand-picked separate by laser fluorination. The latter value is in agreement with the one of +9.4‰ reported by Eiler et al. (1997) for an analysis by conventional vessel fluorination. The two unknown samples yielded laser fluorination values (for 112552-1, +7.07 and 6.63‰; for J-33-D, +9.41 and 9.39‰) that are consistent with one or more ion-microprobe analyses of them, as discussed below. Together, the limited set of ion-microprobe and laser-fluorination data appear to be consistent with independent analysis of standards and each other.

RESULTS

CL observations of jadeitite textures

The CL microstructures show evidence for one or more cycles of crystallization that consist initially of red- or blue-luminescent jadeite, followed by green-luminescent jadeite (Fig. 2). This crystallization sequence of first red or blue, then green is seen in samples from Japan (112552-1), Guatemala (112538), Kazakhstan (102029, 104276), and Burma (BUR-07, CJ-01). Jadeitite from the California locality (J-33-D; Fig. 2b) lacks green luminescence; unlike the other samples, which are extremely compact, J-33-D is a somewhat friable, coarse-grained

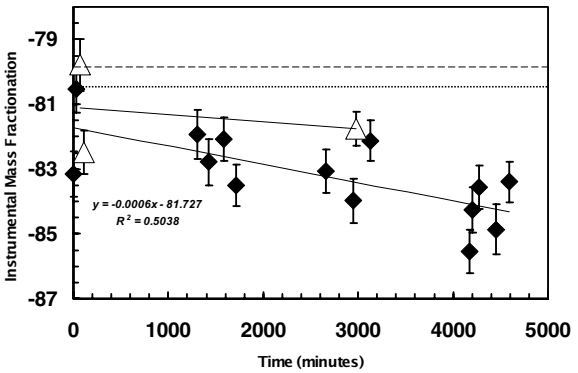

FIGURE 1. Drift corrections, ion microprobe data. Analyses of standards are plotted as follows: triangles, Amelia albite; diamonds, jadeite mineral; both reported in Table 2 of Eiler et al. (1997). The instrumental mass fractionation (IMF) of the Cameca IMS 6f SIMS instrument at the time of analysis at the Carnegie Institution of Washington was significantly offset from that of the Cameca IMS 4f at the University of Edinburgh, with which the Eiler et al. (1997) study was conducted. Accordingly, the data for Amelia albite and albite samples that were collected at ~3000 min elapsed time were drift-corrected to the lowest IMF value obtained for the standard (dashed line). The data for jadeite samples were corrected for drift by the difference between corresponding values on the best-fit line of standard analyses with run time, and the lowest IMF measured for the jadeite standard (dotted line).

vein material, with individual crystals to 3 cm in length and 0.5 cm in diameter.

Jadeitite samples from Japan, Kazakhstan, and Burma show evidence for the partial resorption of blue- and/or red-luminescent jadeite, followed by crystallization of idioblastic green-luminescent jadeitite. This is particularly well-illustrated by Japanese sample 112552-1 (Fig. 2a), which consists of large, idioblastic grains that show irregularly shaped, mottled blue- and red-luminescent cores, which are overgrown by bright- to dull-green luminescent rims. In contrast to the irregularly shaped cores, the grain rims show perfect terminations and oscillatory growth zoning on the millimeter to submicrometer scale. In addition to these two samples, many of the green-luminescent rims seen on the images in Figure 2a appear to have grown without impinging upon other grains, as if into open or fluid-filled space. Kazakh sample 102029 (Fig. 2c) and Burmese sample BUR-07 (Fig. 2d) are other examples of such features. Sample 102029 contains what appears to have once been a "pocket" (center right of image) into which oscillatory zoned, bright- and dark-green-luminescent jadeite has formed a jagged set of grain terminations. Sample BUR-07 (Fig. 2d) displays what appears to be a vein of zoned, bright to dark-green-luminescent, cross-vein jadeite crystals within a matrix of red-blue- to green-luminescent jadeitite. The

TABLE 2. Electron microprobe analyses of jadeite

Sample	CL Color		Index	SiO_2 wt%	TiO_2 wt%	Al_2O_3 wt%	Cr_2O_3 wt%	FeO wt%	MgO wt%	CaO wt%	MnO wt%	BaO wt%
104276												
104276 gr1ln1-6	red	Ca-poorest	15	59.6	0.04	25.8	0.02	0.07	0.04	0.07	0.02	0
104276 gr1ln4-27	red	Ca-richest	93	59.2	0.05	23.6	0.03	0.58	0.96	1.47	0.06	0
104276 Red Avg (43)				59.0	0.05	25.3	0.02	0.09	0.12	0.21	0.03	0.02
104276 gr1ln3-1	blue	Ca-poorest	31	59.3	0.06	25.5	0.04	0.04	0.01	0.06	0.02	0.01
104276 gr2ln3-1	blue	Ca-richest	215	58.1	0.12	19.6	0.07	1.05	4.19	4.25	0.05	0.13
104276 Blue Avg (38)				59.1	0.04	25.1	0.01	0.12	0.25	0.34	0.02	0.02
104276 gr2ln3-3	green	Ca-poorest	217	59.5	0.08	25.2	0.03	0.08	0.16	0.25	0	0.06
104276 gr2ln3-14	green	Ca-richest	228	58.6	0.10	21.1	0.12	0.81	2.66	3.78	0.04	0.03
104276 Green Avg (45)				58.6	0.11	24.0	0.02	0.57	0.90	1.24	0.02	0.03
BUR-07												
BUR-07 ln3-8	red	Ca-poorest	628	59.4	0.03	25.6	0	0.07	0.04	0.07	0.04	0.07
BUR-07 ln3-13	red	Ca-richest	615	59.2	0.04	24.0	0.01	0.46	0.96	1.53	0	0
BUR-07 Red Avg (14)				59.0	0.04	25.1	0.01	0.15	0.22	0.40	0.02	0.02
BUR-07 ln3-15	blue	Ca-poorest	617	59.4	0.04	25.2	0	0.09	0.16	0.23	0	0
BUR-07 ln3-2	blue	Ca-richest	604	58.8	0.17	23.2	0	1.33	1.08	1.43	0.04	0.03
BUR-07 Blue Avg (13)				59.2	0.06	24.9	0.01	0.27	0.32	0.48	0.02	0.02
BUR-07 ln3-12	green	Ca-poorest	614	59.5	0.02	25.4	0	0.04	0.03	0.08	0.01	0
BUR-07 ln3-10	green	Ca-richest	630	58.8	0.10	22.7	0	0.73	1.29	2.49	0.02	0.01
BUR-07 Green Avg (21)				58.8	0.12	23.7	0.01	0.68	0.96	1.45	0.02	0.02
BUR-07 ln3-5	NL	Ca-poorest	607	58.9	0.05	24.9	0.02	0.30	0.32	0.67	0.01	0.04
BUR-07 ln2-1	NL	Ca-richest	565	58.6	0.25	21.6	0.02	1.58	1.73	2.37	0.06	0.02
BUR-07 NL Avg (40)				58.8	0.10	23.9	0.01	0.57	0.85	1.38	0.02	0.02
112538												
112538 gr5ln2-22	red	Ca-poorest	334	59.1	0	25.3	0.01	0.08	0.04	0.13	0.01	0.04
112538 gr2ln3-9	red	Ca-richest	136	59.0	0	24.8	0	0.30	0.45	0.83	0.02	0.01
112538 Red Avg (104)				58.7	0.01	25.4	0	0.11	0.09	0.31	0.02	0.02
112538 gr5 ln1-8	blue	Ca-poorest	257	58.8	0	25.5	0	0.04	0.02	0.18	0.01	0
112538 gr4ln2-26	blue	Ca-richest	218	58.7	0	25.2	0.01	0.21	0.21	0.49	0.02	0
112538 Blue Avg (39)				58.7	0	25.4	0.01	0.04	0.03	0.30	0.01	0.02
112538 gr5ln2-3	green	Ca-poorest	315	58.8	0	25.5	0	0.12	0.01	0.19	0.01	0.03
112538 gr1ln1-7	green	Ca-richest	52	58.0	0.03	23.5	0	0.93	1.22	2.02	0.02	0.05
112538 Green Avg (82)				58.6	0.01	24.4	0.01	0.41	0.58	0.96	0.02	0.02
J-33-D												
J-33-D gr1ln1-1	red	Ca-poorest	13	58.6	0.03	25.7	0.04	0.06	0.02	0.02	0.03	0
J-33-D gr1ln1-13	red	Ca-richest	25	58.4	0.04	25.1	0.02	0.28	0.06	0.36	0.09	0
J-33-D Red Avg (45)				58.4	0.04	25.4	0.01	0.10	0.02	0.11	0.03	0.02
J-33-D gr1ln3-25	blue	Ca-poorest	72	58.2	0.03	25.6	0	0.03	0.02	0.02	0.02	0
J-33-D gr1ln1-14	blue	Ca-richest	26	58.4	0.05	25.1	0.01	0.26	0.03	0.31	0.13	0
J-33-D Blue Avg (48)				58.4	0.03	25.5	0.01	0.04	0.02	0.08	0.02	0.01
112552-1												
112552-1 ln1-22	NI	Ca-poorest	208	57.8	0.07	25.0	0.01	0.22	0.13	0.25	0.01	0
112552-1 ln1-12	NI	Ca-richest	198	57.2	0.03	22.0	0	0.67	2.08	3.02	0.01	0.01
112552 Avg (131)				57.5	0.05	23.5	0.02	0.65	1.01	1.42	0.01	0.01
102029												
102029 ln7-4	NI	Ca-poorest	843	59.4	0	25.6	0.02	0	0	0.04	0	0.03
102029 ln1-1	NI	Ca-richest	584	57.8	0.17	19.4	0.02	1.47	3.50	5.19	0.03	0
102029 Avg (245)				58.8	0.09	23.8	0.02	0.54	1.18	1.73	0.01	0.01
CJ-01												
CJ-01 ln8-1-2	red	Ca-poorest	186	60.0	0.01	25.5	0.01	0.05	0.10	0.12	0	0
CJ-01 ln3-1-3	red	Ca-richest	85	59.3	0.06	24.9	0	0.40	0.37	0.56	0	0
CJ-01 Red Avg (6)				59.8	0.04	25.3	0	0.18	0.25	0.31	0	0
CJ-01 ln1-1-8	blue	Ca-poorest	21	59.1	0.03	25.9	0.02	0.01	0	0	0	0
CJ-01 ln1-1-10	blue	Ca-richest	23	58.3	0.10	23.1	0.01	0.80	1.29	1.76	0	0
CJ-01 Blue Avg (45)				58.6	0.05	24.5	0.01	0.38	0.58	0.94	0.02	0.01
CJ-01 ln1-11-4	green	Ca-poorest	233	59.8	0.02	25.7	0	0.01	0	0.02	0	0
CJ-01-ln5-1-28	green	Ca-richest	141	59.4	0.02	22.6	0.01	0.72	1.82	2.50	0	0
CJ-01 Green Avg (138)				59.3	0.07	23.9	0.01	0.65	0.96	1.31	0	0

Notes: NL = non-luminescent; NI = not indexed.

oscillatory zoning of such grains is common, and occurs on scales of <1 µm. As noted above, California jadeitite J-33-D (Fig. 2b) contains large prismatic grains that display literally thousands of oscillations between red- and blue-luminescent jadeite. In the other images, most green-luminescent jadeite shows oscillations between brighter and darker green colors. Irregularly shaped green-luminescent rims upon blue- and/or red-luminescent jadeite grains are found in samples from Guatemala (Fig. 2f) and Kazakhstan (Fig. 2g); the latter also shows ~0.2 mm, fractured green-luminescent jadeite veins, cut by veins of nonluminescent jadeite hundreds of micrometers thick.

Other than the California jadeitite only one sample appears to violate "red or blue, followed by green" crystallization sequence: CJ-01 (Fig. 2e), from Nansibon, Burma. The veins in

TABLE 2.—*Extended*

Na2O wt%	Total wt%	Si	Ti	Al	Cr	Fe^{2+}	Fe^{3+} (est)	Mg	Ca	Mn	Ba	Na	(Na+Ca)	Octa-hedral Σ	Tetra-hedral Σ	Total
15.4	99.87	1.99	0	1.01	0	0	0	0	0	0	0	1.00	1.00	2.02	1.99	4.00
14.5	99.45	2.00	0	0.94	0	0	0.01	0.05	0.05	0	0	0.94	1.00	2.00	2.00	4.00
15.2	98.97	1.99	0	1.01	0	0	0	0.01	0.01	0	0	0.99	1.00	2.02	1.99	4.00
15.5	99.33	1.99	0	1.01	0	0	0	0	0	0	0	1.01	1.01	2.02	1.99	4.01
12.1	98.75	1.99	0	0.79	0	0.02	0.01	0.21	0.16	0	0	0.80	0.96	2.01	1.99	4.00
15.0	98.95	1.99	0	1.00	0	0	0	0.01	0.01	0	0	0.98	0.99	2.01	1.99	4.00
15.1	99.36	1.99	0	1.00	0	0	0	0.01	0.01	0	0	0.98	0.99	2.00	1.99	4.00
13.1	99.36	1.99	0	0.84	0	0	0.02	0.13	0.14	0	0	0.87	1.00	2.01	1.99	4.00
14.5	98.92	1.98	0	0.96	0	0	0.02	0.05	0.05	0	0	0.95	1.00	2.02	1.99	4.00
15.2	99.38	1.99	0	1.01	0	0	0	0	0	0	0	0.99	0.99	2.01	1.99	4.00
14.5	99.56	1.99	0	0.95	0	0	0.01	0.05	0.06	0	0	0.95	1.00	2.01	1.99	4.00
15.0	98.89	1.99	0	1.00	0	0	0	0.01	0.01	0	0	0.98	1.00	2.01	1.99	4.00
15.2	99.32	1.99	0	1.00	0	0	0	0.01	0.01	0	0	0.99	1.00	2.01	1.99	4.00
14.2	99.33	1.99	0	0.93	0	0.02	0.02	0.05	0.05	0	0	0.93	0.99	2.01	1.99	4.00
15.0	99.16	1.99	0	0.99	0	0	0.01	0.02	0.02	0	0	0.98	0.99	2.01	1.99	4.00
15.4	99.38	1.99	0	1.00	0	0	0	0	0	0	0	1.00	1.01	2.01	1.99	4.01
14.3	99.39	1.99	0	0.91	0	0	0.02	0.07	0.09	0	0	0.94	1.03	2.03	1.99	4.02
14.4	99.03	1.99	0	0.94	0	0.01	0.01	0.05	0.05	0	0	0.94	1.00	2.01	1.99	4.00
14.7	98.92	1.99	0	0.99	0	0.01	0	0.02	0.02	0	0	0.97	0.99	2.01	1.99	4.00
13.9	99.08	1.99	0.01	0.87	0	0	0.04	0.09	0.09	0	0	0.92	1.01	2.02	2.00	4.00
14.3	98.97	1.99	0	0.96	0	0.01	0	0.04	0.05	0	0	0.94	0.99	2.01	1.99	4.00
14.6	99.32	2.00	0	1.01	0	0	0	0	0	0	0	0.96	0.96	2.01	2.00	3.98
14.2	99.60	2.00	0	0.99	0	0.01	0	0.02	0.03	0	0	0.93	0.96	2.01	2.00	3.98
14.6	99.20	1.99	0	1.01	0	0	0	0	0.01	0	0	0.96	0.97	2.01	1.99	3.98
14.6	99.22	1.99	0	1.02	0	0	0	0	0.01	0	0	0.96	0.97	2.01	1.99	3.98
14.5	99.35	1.99	0	1.01	0	0.01	0	0.01	0.02	0	0	0.95	0.97	2.01	1.99	3.98
14.7	99.18	1.99	0	1.01	0	0	0	0	0.01	0	0	0.96	0.98	2.01	1.99	3.98
15.0	99.60	1.99	0	1.02	0	0	0	0	0.01	0	0	0.98	0.99	2.01	1.99	4.00
13.6	99.33	1.98	0	0.95	0	0.03	0	0.06	0.07	0	0	0.90	0.97	2.01	1.98	3.99
14.2	99.24	1.99	0	0.98	0	0.01	0	0.03	0.04	0	0	0.94	0.97	2.01	1.99	3.99
14.6	99.08	1.99	0	1.03	0	0	0	0	0	0	0	0.96	0.96	2.01	1.99	3.98
14.4	98.67	1.99	0	1.01	0	0.01	0	0	0.01	0	0	0.95	0.97	2.01	1.99	3.98
14.6	98.77	1.99	0	1.02	0	0	0	0	0	0	0	0.96	0.96	2.01	1.99	3.98
14.5	98.39	1.99	0	1.03	0	0	0	0	0	0	0	0.96	0.96	2.01	1.99	3.98
14.5	98.82	1.99	0	1.01	0	0.01	0	0	0.01	0	0	0.96	0.97	2.01	1.99	3.98
14.6	98.73	1.99	0	1.02	0	0	0	0	0	0	0	0.96	0.96	2.01	1.99	3.98
14.5	98.05	1.98	0	1.01	0	0.01	0	0.01	0.01	0	0	0.97	0.98	2.01	1.98	3.99
12.9	97.78	1.99	0	0.90	0	0.02	0	0.11	0.11	0	0	0.87	0.98	2.01	1.99	4.00
13.9	98.13	1.99	0	0.96	0	0.02	0	0.05	0.05	0	0	0.93	0.99	2.01	1.99	4.00
15.0	100.03	2.00	0	1.01	0	0	0	0	0	0	0	0.97	0.98	1.99	2.00	3.99
11.9	99.41	2.00	0	0.79	0	0.04	0	0.18	0.19	0	0	0.79	0.99	2.00	2.00	4.00
14.3	100.38	1.98	0	0.95	0	0	0.02	0.06	0.06	0	0	0.93	1.00	2.02	1.98	4.00
15.0	100.87	2.00	0	1.00	0	0	0	0	0	0	0	0.97	0.97	1.98	1.98	3.98
15.1	100.66	1.99	0	0.98	0	0	0.01	0.02	0.02	0	0	0.98	1.00	2.02	2.01	4.01
15.2	101.03	1.99	0	0.99	0	0	0	0.01	0.01	0	0	0.98	1.00	2.01	2.00	4.00
15.0	100.07	1.98	0	1.03	0	0	0	0	0	0	0	0.98	0.98	2.01	1.99	3.99
14.1	99.54	1.99	0	0.93	0	0	0.02	0.07	0.06	0	0	0.93	1.00	2.02	2.01	4.00
14.4	99.28	1.99	0	0.98	0	0.01	0	0.03	0.03	0	0	0.95	0.98	2.01	1.99	3.99
15.4	100.94	1.99	0	1.01	0	0	0	0	0	0	0	1.00	1.00	2.01	2.00	4.00
13.8	100.89	2.00	0	0.90	0	0.01	0.01	0.09	0.09	0	0	0.90	0.99	2.00	2.00	4.00
14.5	100.81	1.99	0	0.95	0	0.01	0	0.05	0.05	0	0	0.95	0.99	2.01	2.00	4.00

sample CJ-01, which overgrow a population of largely resorbed blue-red-luminescent jadeite grains, consist of yellow-green-luminescent jadeite that is progressively zoned to blue and red rims. In the lower right corner of Figure 2e, the corroded grain cores of red-blue jadeite are apparent; away from the veins, the rock matrix that the veins cut consists of unresorbed red- and blue-luminescent jadeite grains. Overall, the oscillatory zoned, green-luminescent vein jadeite of CJ-01 clearly postdates resorption of red-blue-luminescent matrix jadeite, whereas the blue and red luminescent rims on the yellow-green luminescent vein-forming grains apparently records the inception of yet another "blue/red to green" crystallization cycle.

TABLE 3. SIMS trace element analyses of jadeitite samples

Sample name	CL	SEQ	Li ppm	Be ppm	Sc ppm	Ti ppm	Cr ppm	Rb ppm	Sr ppm	Y ppm	Zr ppm
Guatemala											
112538-R1	Red	1	91	0	26	76	4.8	0	2.0	0.21	0
112538-R2	Red	1	96	0	24	0	0	0	0	0.17	0
112538-B1	Blue	1	82	0.10	25	0	3.9	0	0	0	0
112538-B2	Blue	1	83	0.10	26	0	4.1	0	0	0	0
112538-B3	Blue	1	78	0.15	25	0	5.4	0	0	0.10	0
112538-G1	Green	2	102	0.31	25	151	12	0.23	4.1	0.22	1.0
112538-G2	Green	2	73	0.03	24	56	9.3	0	1.0	0	0
112538-G2-98	Green	2	61	1.7	18	0	7.8	0	0	0.10	0
Japan											
112552-1-R1	Red	1	33	0.32	24	0	8.1	0.2	0	0	3.5
112552-1-R2	Red	1	31	0.22	28	0	10	0.3	7.2	0.25	7.9
112552-1-B1	Blue	2	22	0.41	25	0	0	2.3	0	0	3.2
112552-1-G1	Green	3	25	0.88	25	153	22	0.2	29	0.51	34
112552-1-G2	Green	4	31	0.42	27	145	314	0.2	41	0.80	33
California											
J33D-NL1	NL	1	20	2.1	27	0	3.5	0	0	0	0
J33D-R1	Red	2	13	2.8	25	118	3.2	0.08	0	0	11
J33D-R2	Red	3	7.3	2.1	26	0	2.7	0	0	0	11
J33D-B1	Blue	4	10	2.0	28	0	3.8	0	0	0	0
Burma											
CJ-01 DG	Green	1	76	0	8.4	258	1.9	0	3.9	0.31	92
CJ-01 DG	Green	2	109	0.04	26	277	9.4	0.23	8.7	0.57	90
CJ-01 BG	Green	3	110	0.03	26	248	12	0.25	13	0.79	75
CJ-01 BG	Green	4	123	0.04	25	399	16	0.36	16	0.65	27
CJ-01 DG	Green	5	115	0.05	25	520	19	0.43	9.4	0.56	20
CJ-01 B	Blue	6	108	0	24	20	4.8	0	0	0.16	5.8
CJ-01 B	Blue	6	66	0.11	25	54	0	0.13	5.9	0.16	4.1
CJ-01 B	Blue	7	26	0.05	25	0	3.9	0	0	0	0
CJ-01 B	Blue	8	30	0.07	25	0	3.4	0	0	0	0
Burma											
BUR07-R1	Red	1	29	1.7	24	178	6.6	0.07	0	0.32	0.67
BUR07-B1	Blue	2	19	1.7	24	0	5.1	0	0	0.27	0.0
BUR07-G3	Green	3	26	1.5	24	259	14	0.27	34	0.76	10
BUR07-G1	Green	4	21	1.6	23	3445	18	0.21	33	2.8	26
BUR07-G2	Green	5	22	1.5	23	386	20	0.22	4.2	1.2	1.1
Kazkahstan											
102029-RB1	R/B	1	23	3.5	13	688	36	0.33	13	1.7	21
102029-G1	Green	2	24	3.3	12	544	11	0.18	0	0.90	1.5
102029-NL	NL	3	20	4.1	12	188	6.9	0.08	0	0.34	0.43
102029-SZ1	Green	4	22	3.3	14	312	79	0.22	27	2.3	19
Kazkahstan											
104276-B1	Blue	1	11	0.39	27	0	3.4	0	0	0.0	2.2
104276-B2	Blue	1	32	0.23	27	0	5.5	0	0	0.42	16
104276-R1	Red	2	0	0.30	26	0	3.7	0	0	0.74	0.90
104276-G2	Green	3	17	0.35	26	382	214	0.38	0	1.6	3.0
104276-G1	Green	4	14	0.22	28	573	269	0.86	124	10	76

Electron microprobe analyses of jadeite compositions

Approximately 1000 electron microprobe analyses of jadeite grains in the seven samples (summarized in Table 2) show that the principal major- and minor-element substitutions are: diopside ($Na^{+}\ {}^{VI}Al^{3+} \rightarrow Ca^{2+}\ {}^{VI}Mg^{2+}$), Fe-Mg exchange (${}^{VI}Mg^{2+} \rightarrow {}^{VI}Fe^{2+}$) and aegirine (here, ${}^{VI}Al^{3+} \rightarrow {}^{VI}Fe^{3+}$). Although the aegirine substitution is probably less significant than Fe-Mg exchange, the former is somewhat challenging to assess. The ratio Fe^{2+}/Fe^{3+} is difficult to estimate for these analyses by combining electron microprobe analyses with stoichiometric constraints, owing to the relatively small amounts of total Fe (as FeO) present in the grains and the errors associated with the analytical technique. In Table 2, many analyses total less than 4.00 cations (normalized to 6 O atoms). This means that estimating Fe^{3+}/Fe^{2+} by mathematically converting Fe^{2+} to Fe^{3+} cations (and thus lowering cation sums >4 to that value) for a 6 oxygen pyroxene formula is impossible. With this caveat, many aspects of the minor-element chemistry of these jadeites—and their possible ramifications for the state of Fe in the grains—can be examined.

The jadeite grains are slightly to strongly zoned in major- and minor-element compositions. Figure 3 shows the microprobe mineral compositions of multiple traverses of five jadeite grains from sample 112538, a jadeitite-albitite rock from Guatemala. CL images (e.g., Fig. 2f) show red- and/or blue-luminescent grain cores and green-luminescent grain rims. The latter, shown as downward-pointing triangles in Figure 3, are significantly richer in Fe, Mg, and Ca than cores. Indeed, the green-luminescent grain rims in sample 112538 show up to 7% diopside solid solution (Fig. 3). Overall, green-luminescent or non-luminescent zones within jadeite grains in this sample suite show a maximum of 10% of a diopside solid solution (Table 2). In Figure 4, evidence for the predominance of diopside solid solution is based primarily on the nearly 1:1 correlations of Ca and Mg cations in the formula (Fig. 4a), albeit at a ratio slightly less than 1. Therefore, a small amount of Fe^{2+} (i.e., a hedenbergite component) is required, along with diopside, to explain the Ca-clinopyroxene substitutions for jadeite. The amount of Fe^{2+} that is nominally available in the analyses is more than adequate to do this (Fig. 4b). Although

TABLE 3.—*Extended*

Hf ppm	Nb ppm	Ba ppm	La ppm	Ce ppm	Nd ppm	Sm ppm	Eu ppm	Gd ppm	Dy ppm	Er ppm	Yb ppm
0.04	0.04	2.8	0	3.0	2.4	0	1.1	0	0	0	0.03
0	0	3.5	0	0.02	0	0	0.01	0	0	0	0
0	0	0	0	0	0	0	0	0	0	0	0
0	0	0	0	0	0	0	0	0	0	0	0
0	0.02	0	0	0	0	0	0	0	0	0	0
0	0.03	0	0	0	0	0	0.09	0	0	0	0
0	0	0	0	0	0	0	0	0	0	0	0
0	0	0	0	0	0	0	0	0	0	0	0
0.10	0	0	0	0	0	0	0	0	0	0	0
0.20	0.05	0	0.14	0	0.08	0	0	0.02	0.02	0.01	0
0	0	0	0	0	0	0.02	0	0.02	0	0	0
0.89	0	0	0	0	0.16	0	0.04	0.1	0	0.1	0.03
0.72	0.03	0	0.03	0.12	0.24	0.09	0.06	0.10	0.10	0.06	0.06
0	1.3	0	0	0	0	0	0	0	0	0	0
0	1.5	0	0	0	0	0	0	0	0	0	0
0.08	2.2	0	0	0	0	0	0	0	0	0	0
0	79	0	0	0	0	0	0	0	0	0	0
2.7	0.01	0	0	0.03	0.06	0	0	0	0	0.1	0.1
2.9	0.02	0	0	0	0.17	0.09	0.03	0.05	0	0	0
2.5	0.02	0	0	0	0	0.11	0.04	0.09	0.12	0.10	0.11
0.74	0	0	0	0.18	0.23	0.11	0.04	0.09	0.09	0.08	0.09
0.79	0.03	0	0	0.18	0.24	0.10	0.04	0.07	0.10	0.08	0.07
0	0	0	0	0	0	0.05	0	0	0	0	0
0.24	0	0	0	0	0	0	0	0	0	0.04	0
0	0	0	0	0	0	0	0	0	0	0	0
0	0	0	0	0	0	0	0.10	0	0.03	0	0
0	4.7	0	0	0	0.15	0	0	0.06	0	0	0
0	5.3	0	0	0	0.16	0	0	0	0	0	0
2.1	0.67	1165	0.25	0.41	0.33	0	1.2	0.19	0.51	0	0.10
0.21	11	12.5	0.77	2.6	2.2	0.80	0.31	0.77	0.52	0.18	0.11
0	0.45	0	0	0.36	0.34	0.17	0.07	0.17	0.19	0.07	0.04
0.24	0.35	3.4	0.22	0.70	0.79	0.30	0.14	0.32	0.27	0.13	0.13
0	0.26	0	0.17	0.39	0.27	0.11	0.05	0.11	0.12	0.06	0
0	0.07	0	0	0.03	0	0	0.01	0	0	0	0
0.59	1.0	6.4	0.44	1.3	1.5	0.51	0.21	0.41	0.35	0.14	0.13
0	0.06	0	0	0	0	0	0	0	0	0	0
0.44	25	0	0	0	0	0	0	0.1	0	0	0
0	0.73	0	2.2	3.5	1.2	0.18	0.06	0.20	0.08	0.07	0.05
0.80	0	0	0	0	0	0.17	0	0.20	0.20	0.08	0.04
1.5	1.1	0	3.2	6.5	4.3	1.6	0.75	1.6	1.6	0.80	0.72

Figure 4 also shows that small amounts of the diopside substitution are detectable—perhaps because the grains contain little else—at $X_{Ca} < 0.015$, the correlation appears to break down (Fig. 4b). This finding likely reflects scatter produced by errors in the measurements of such miniscule amounts of Ca and Mg.

Trace-element contents of jadeitite

The distribution of CL colors and intensities within a luminescent mineral grain or specimen maps spatial and temporal variations of the minor and trace elements that both activate or are correlated with different colors of luminescence (Marshall 1988; Pagel et al. 2000). The crystal chemistry of jadeite suggests that CL could be activated by a large number of possible cation substitutions. The tetrahedral site of this pyroxene is occupied almost exclusively by Si, but both the M1 (nominally Al^{3+}, but commonly Fe^{3+}, Cr^{3+}, etc.) octahedra and M2 (nominally Na^{+}, but commonly Li^{+}) 8-coordinated polyhedra yield charge-balanced solid solutions to aegirine, kosmochlor, and spodumene, among other end-members. In addition, the incorporation of major elements via the diopside-hedenbergite substitution:

$$^{M2}Na^{+} + {}^{M1}Al^{3+} \rightarrow {}^{M2}Ca^{2+} + {}^{M1}(Mg,Fe^{2+})$$

yields omphacite- or augite structural positions that by charge and/or increased ionic radius, permit the substitution of trace amounts of many transition metals and the REE. Some of these, such as Fe^{2+} or Fe^{3+}, Mn^{2+}, and REE^{3+}, are known CL activators in both feldspar and pyroxene (e.g., Marshall 1988; Pagel et al. 2000). However, many other trace elements may be accommodated in the same sites as are CL-activators. We did not attempt to identify the specific activators responsible for the CL of jadeite grains. Instead, we used CL images as generalized "trace-element maps" of the jadeitites to guide analysis by secondary ion mass spectrometry (SIMS; the ion microprobe).

Comparison of Li-contents of samples for which CL-color-indexed data were collected shows that this element, which, owing to solid solution with spodumene ($LiAlSi_2O_6$) is likely to be compatible during crystallization, shows no systematic behavior from locality to locality (Fig. 5). The abundance and isotopic composition of Li can monitor fluid-rock interactions in subduction zones (Berger et al. 1988; Seyfried et al. 1998;

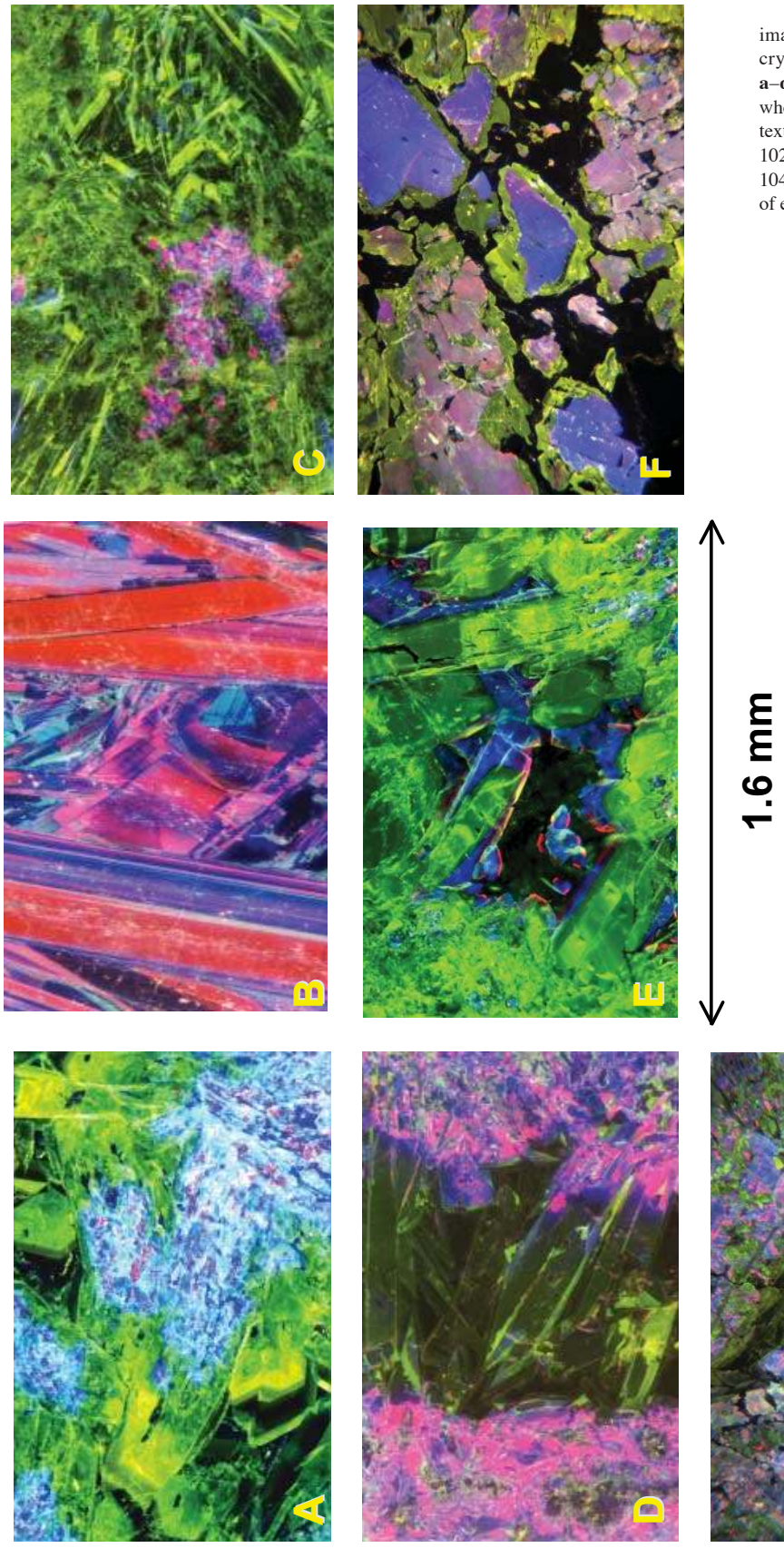

FIGURE 2. Cathodoluminesence (CL) images of jadeitite, showing the varieties of crystallization textures seen in CL. Images **a–d** captured by conventional photography, whereas **e–g** are processed CCD images (see text). Samples are: (**a**) 112552-1; (**b**) J-33-D; (**c**) 102029; (**d**) BUR-07; (**e**) CJ-01; (**f**) 112538; (**g**) 104276. See text for further discussion. (Width of each image is 1.6 mm.)

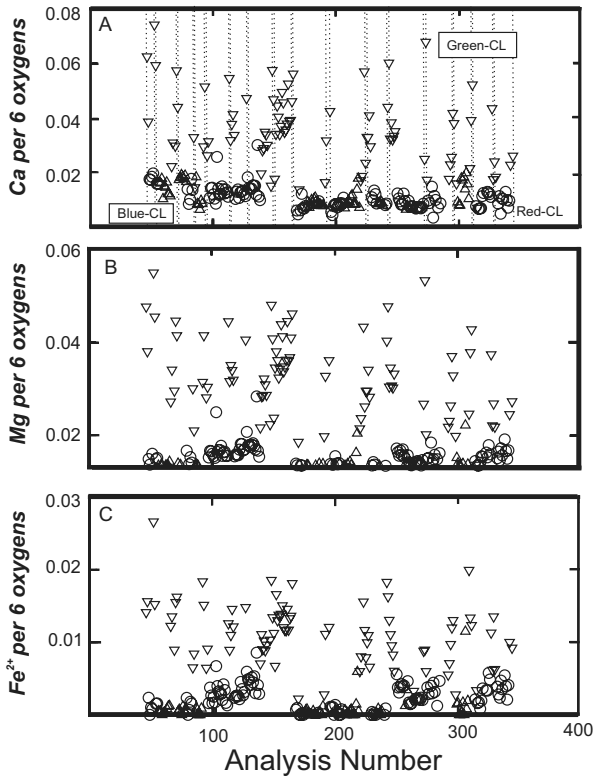

FIGURE 3. Formula contents of Ca, Mg, and Fe^{2+} in jadeite, sample 112538. These are data for sixteen rim-core-rim line traverses of five different grains within the sample. The beginning and end of each traverse (i.e., rim analyses) are designated by vertical dotted lines in **a**. The symbols refer to the cathodoluminescence (CL) colors at each analysis point, which are as follows: circle = red CL; upward pointing triangle = blue CL; and the downward pointing triangle = green CL. The Fe^{2+} and Fe^{3+} contents of jadeite were estimated by normalizing microprobe analyses to both 6 O atoms and 4 cations. This estimate for Fe^{2+} is small, and likely within the errors of the microprobe analysis, which raises the possibility that all the Fe in these samples is Fe^{3+}. This problem is discussed further in the caption for Figure 4.

Brenan et al.; 1998; Chan et al. 1999; Zack et al. 2003; Elliott et al. 2004). Subducted sediment is thought to be the principal reservoir rock, because white mica (which has the Li end-member, lepidolite) can host weight percent quantities of the element. The Li contents of jadeite in these samples range from 7.3 to 123 ppm (Table 3). The latter is a relatively large value for a

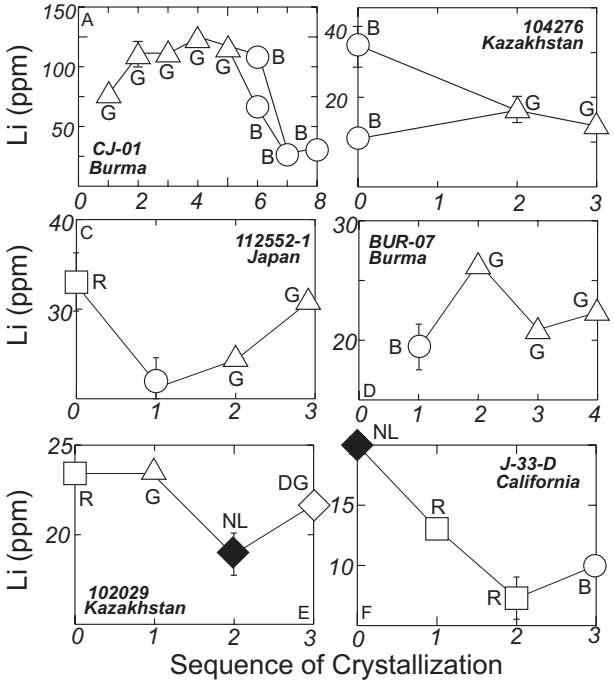

FIGURE 5. Li-contents (ppm) of jadeitites. The symbols are: upward pointing triangles = green CL jadeite; circles = blue CL jadeite; squares = red-luminescent jadeite; and diamonds = non-luminescent jadeite. The error bars shown on a single point in each plot are representative of the of that data set as a whole. Each plot shows a different range for Li. The X-axis shows numbers that represent the relative time of crystallization of each color-type, from early (0) to late (3–8). Li-contents of sample 112538 are discussed in the text but not plotted.

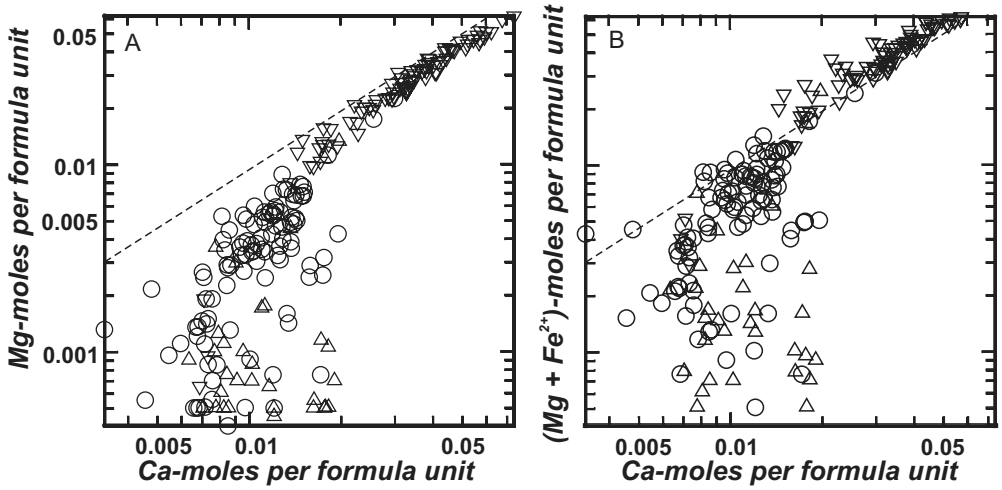

FIGURE 4. Moles of (**a**) Ca vs. Mg, and (**b**) Ca vs. (Mg + Fe^{2+}) in jadeite, sample 112538. These ~300 analyses of 5 grains in the sample show evidence for both diopside-jadeite solid solution and a hedenbergite ($CaFe^{2+}$) substitution. The preponderance of Ca^{2+} substitution for Na^{+} is evidently charge-balanced by Mg^{2+} for Al^{3+} (**a**), but a small amount of Fe^{2+} is arguably present in samples with 0.008 to 0.017 Ca-moles per formula unit (**b**). The sum (Mg + Fe^{2+}) shows a small excess over Ca in the range of Ca = 0.02 to 0.05. Either some of the Fe calculated by the 6 oxygen, 4 cation normalization to be Fe^{2+} is in fact Fe^{3+}, or an extremely small augite component is also present.

sodic clinopyroxene (e.g., Zack et al. 2003). Despite obvious large variations of Li content, and likely, therefore, Li supply, during crystallization of the jadeitites (Fig. 5), there is no overall correlation between CL color and the Li-content of jadeite. (And of course, Li does not activate CL.) However, this lack of correlation also shows that the substitution of small amounts of diopside evidently does not markedly affect the ability of Na-Al rich pyroxene to accommodate trace to minor amounts of Li, as is evidenced by the Li-contents of omphacite in eclogite (up to 64 ppm; Zack et al. 2003).

Overall, both the Li and other trace-element data show within-sample, and in some cases, within grain variations of elements with different geochemical and crystal-chemical properties (Table 3). Trace-element abundances vary widely between and within the samples (Table 3, Figs. 5 and 6). In most samples, trace-element abundances may vary among the different CL zones of each sample or grain. This is seen in Figure 6, which shows elemental values vs. the crystallization order of each CL-color zone within the sample.

Green-luminescent jadeite, which, as noted above, is richer in a diopside-hedenbergite component than red- or blue-luminescent jadeite, is also in general relatively rich in trace ele-

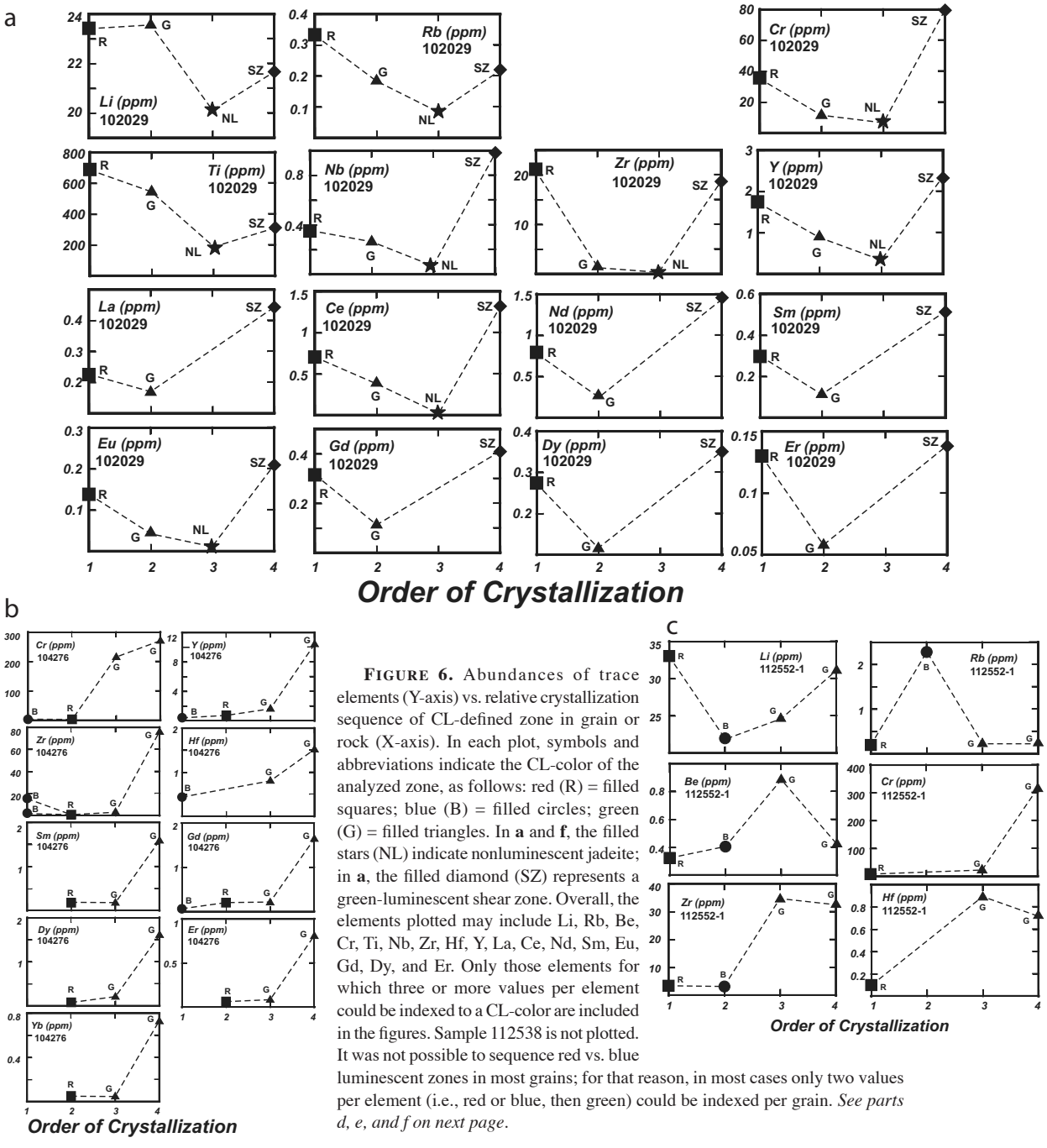

FIGURE 6. Abundances of trace elements (Y-axis) vs. relative crystallization sequence of CL-defined zone in grain or rock (X-axis). In each plot, symbols and abbreviations indicate the CL-color of the analyzed zone, as follows: red (R) = filled squares; blue (B) = filled circles; green (G) = filled triangles. In **a** and **f**, the filled stars (NL) indicate nonluminescent jadeite; in **a**, the filled diamond (SZ) represents a green-luminescent shear zone. Overall, the elements plotted may include Li, Rb, Be, Cr, Ti, Nb, Zr, Hf, Y, La, Ce, Nd, Sm, Eu, Gd, Dy, and Er. Only those elements for which three or more values per element could be indexed to a CL-color are included in the figures. Sample 112538 is not plotted. It was not possible to sequence red vs. blue luminescent zones in most grains; for that reason, in most cases only two values per element (i.e., red or blue, then green) could be indexed per grain. *See parts d, e, and f on next page.*

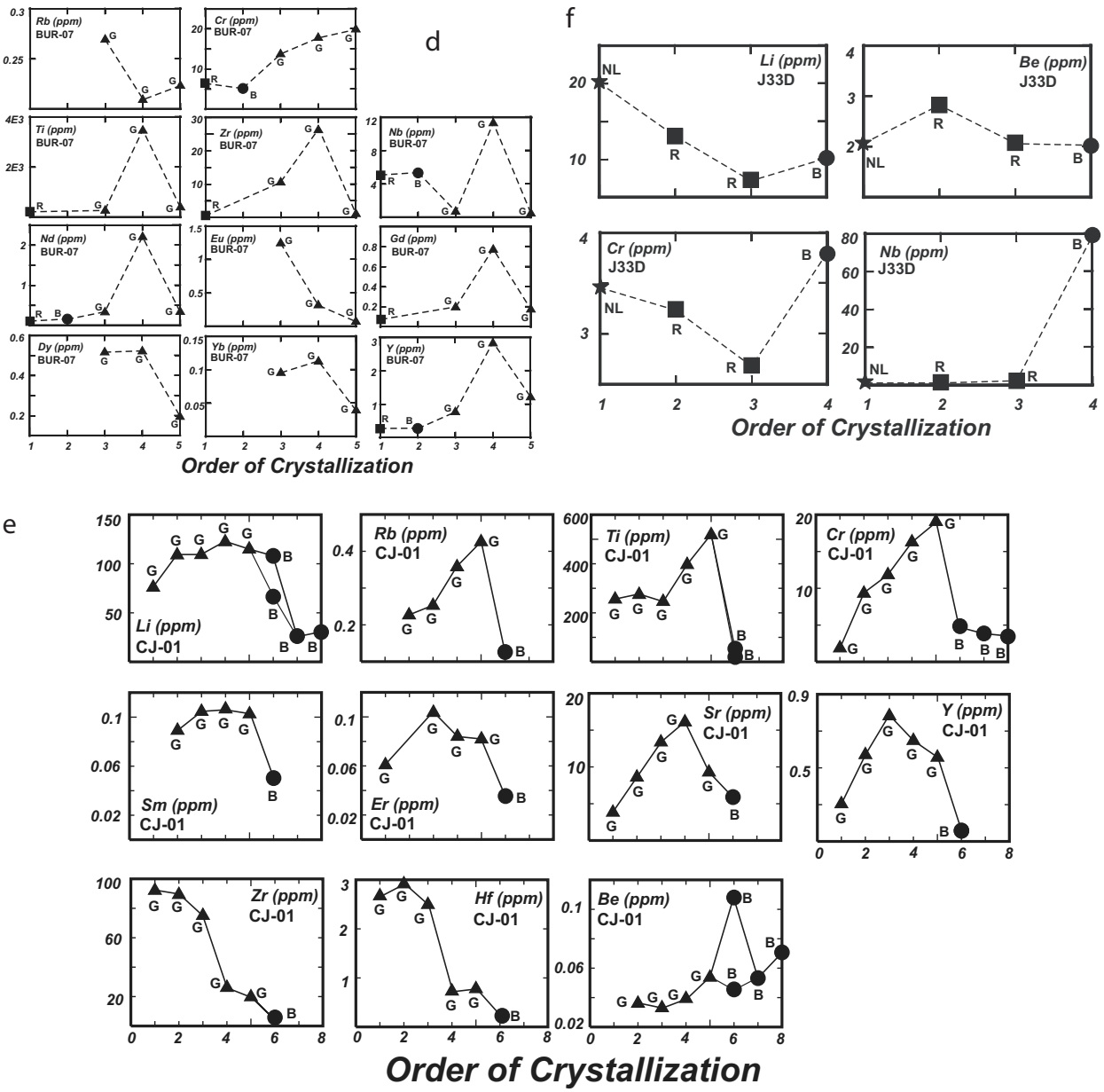

ments, and particularly the REE (Table 3). This feature might be ascribed to a crystal-chemical effect (i.e., minor amounts of Ca substitution for Na, and Mg and Fe^{2+} substitution for Al in jadeite might also create more favorable environments for substitution of transition metals and REE). However, some samples are uniformly poor in trace elements, CL color notwithstanding. For example, rare earth elements (REE) are, for the most part, below the parts-per-billion-to-trillion detection limits of the ion microprobe in analyses of samples 112538, 112552-1, and J-33-D (Table 3, Fig. 6). Samples 112538 and 112552-1 both consist at least in part of green-luminescent jadeite, which is REE-poor in these samples. Individual samples of jadeitite evidently have the capacity to record different histories of trace element supply to them. If this is the case, to which process(es) does each of the seven samples testify?

Sample 102029, from Kazakhstan, appears to have progressed from red-, to green-, to non-luminescent jadeite; it also shows a shear zone of green-luminescent jadeite—in which CL growth structures have apparently been eradicated—that cuts all of the other zones (Fig. 2c). Most trace elements (Table 3, Fig. 6a) are depleted during the primary crystallization sequence but enriched in the late shear zone. Sample 104276, also from Kazakhstan, shows a basic structure of rounded blue- and red-luminescent grains (Fig. 2g). In this sample, red-luminescent jadeite appears to postdate blue, and the grains are rimmed by green-luminescent jadeite. The blue- and red-luminescent jadeite is trace-element poor, but green-luminescent grain rims record the presence of Cr-, Zr-, and REE (+Y; Fig. 6b). Sample 112552-1, from the Omi-Kotaki district of Japan, shows mottled, corroded appearing cores of blue- and red-luminescent jadeite. These are overgrown

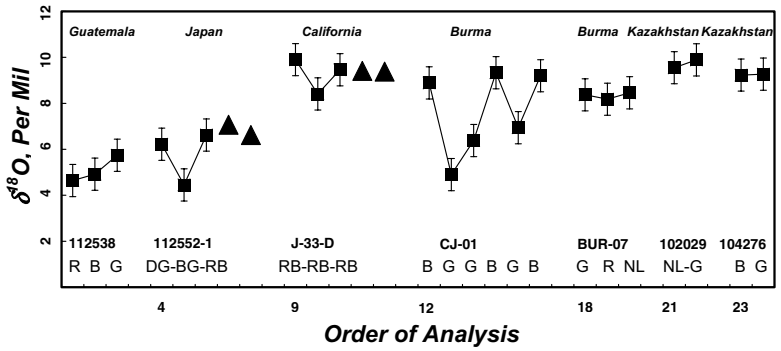

FIGURE 7. Values of $\delta^{18}O$, by ion microprobe, vs. order of analysis. Each sample shows a group label, and samples are separated by one unit. Error bars are ±0.7 per mil; this reflects a 1 σ error average for the ion microprobe data. Four analyses by laser fluorination are also shown as filled triangles. The errors associated with these data are about the size of the points themselves. Abbreviations for CL colors are: R = red; B = blue; G = green; DG = dull or dark green; BG = bright green; RB = purple or intermixed red and blue; Y = bright yellow-green; and NL = non-luminescent.

TABLE 4. Drift corrected oxygen isotope values (δ18O, ‰) for jadeitite samples

Sample	δ18O, ‰	1σ error, ‰			
112538 Red CL	4.6	0.7			
112538 Blue CL	4.9	0.7			
112538 Green CL	5.7	0.6			
112552-1 Dark Green CL	6.2	0.6			
112552-1 Bright Green CL	4.5	0.7			
112552-1 Red/Blue CL	6.6	0.7			
112552-1 Rumble 1	7.1	0.1			
112552-1 Rumble 2	6.7	0.1			
J-33-D Red/Blue CL	9.9	0.7			
J-33-D Red/Blue CL	8.4	0.6			
J-33-D Red/Blue CL	9.5	0.6			
J-33-D Rumble 1	9.4	0.1			
J-33-D Rumble 2	9.4	0.1			
			Reorganized by crystallization sequence		
				δ18O, ‰	1σ error, ‰
CJ-01 Blue CL	8.9	0.6	CJ-01 Yellow 1 CL	4.9	0.6
CJ-01 Yellow 1 CL	4.9	0.6	CJ-01 Yellow 2 CL	6.4	0.6
CJ-01 Yellow 2 CL	6.4	0.6	CJ-01 Yellow 3 CL	6.9	0.7
CJ-01 Blue 2 CL	9.3	0.6	CJ-01 Blue CL	8.9	0.6
CJ-01 Yellow 3 CL	6.9	0.7	CJ-01 Blue 2 CL	9.3	0.6
CJ-01 Blue 3 CL	9.2	0.6	CJ-01 Blue 3 CL	9.2	0.6
CJ-01 Albite	11.9	0.6			
BUR07 Green CL	8.4	0.6			
BUR07 Red CL	8.2	0.8			
BUR07 NonLuminescent	8.5	0.7			
102029 NonLuminescent	9.6	0.7			
102029 Green-CL Shear Zone	9.9	0.8			
112538 Albite	12.3	0.7			
104276 Blue CL	9.2	0.8			
104276 Green CL	9.3	0.7			

Note: Samples listed in order of analysis, except for those analyzed by D. Rumble, III.

by idioblastic, zoned green-luminescent jadeite (Fig. 3a), some of which shows oscillatory zoning. Both Li and Cr rise in abundance as grains crystallize (Fig. 6c). In contrast, Be, Zr, and Hf all reach their maximum abundances within green-luminescent zones and then decrease. Rb reaches a maximum abundance of about 2.5 ppm in the blue-luminescent zone (Fig. 6c). Sample BUR-07 is a granular red- and blue-luminescent jadeitite in which blue-luminescent zones postdate red ones. This rock is cut by a coarse-grained vein of idioblastic, dull- to bright-green-luminescent crystals (Fig. 2d). The latter show evidence for a fluid that was rich in HFSE and REE during grain growth. In contrast to this "spike" of trace elements, Cr appears to have steadily increased during jadeite growth in BUR-07 (Fig. 6d). The CL and trace-element zoning of sample CJ-01 (Figs. 2e and 6e) is discussed in detail below. In that sample, oxygen-isotope zoning is correlated with the trace-element zoning. Finally, although sample J-33-D lacks both abundant trace elements and green-luminescent jadeite, it varies from 20 to 7.3 ppm in Li, the latter being the least amount measured in this study (Fig. 6f).

Oxygen-isotope systematics of jadeitites

As is the case for trace elements, the $\delta^{18}O$ values of jadeite varied widely within and among the samples. Two of the seven samples had $\delta^{18}O$ values <+7‰, four had values >+8‰, and one ranged from +4.90 to 9.33‰. Corrected values for $\delta^{18}O$ in jadeite from the samples are plotted in Figure 7 vs. the order of analysis. Four $\delta^{18}O$ analyses obtained by laser fluorination of hand-picked grains are also illustrated in the figure. Two of these are from sample 112552-1 (Japan), and two are from sample J-33-D (California; Table 4). The agreement between the laser-fluorination results and those determined by SIMS indicates that the lighter values do not reflect systematic instrument biases or drift. (The SIMS data were corrected for instrumental drift, as described above.) This drift-corrected data set shows $\delta^{18}O$ values that range from +4.45 to 9.89‰ (Table 4, Fig. 7), an overall span of 5.44‰. The $\delta^{18}O$ values of the CL zones of four samples (J-33-D, BUR-07, 102029, and 104276) do not change in a statistically significant way with CL color. All four of these samples show $\delta^{18}O$ values of +8.18 to 9.89‰ (Table 4, Fig. 7). Three samples show conspicuous variations of $\delta^{18}O$ values, which are correlated with CL. Guatemalan jadeitite sample 112538 displays red- and blue-luminescent grain cores with $\delta^{18}O$ values of +4.64 and 4.92‰, respectively. The more omphacitic, green-luminescent grain rim shows a $\delta^{18}O$ value of +5.74‰. In this sample, it appears as if the late-stage, green-luminescent jadeite is slightly heavier than the red- or blue-luminescent predecessor. Japanese jadeitite sample 112552-1 shows a different oxygen-isotope zoning trend. It displays a $\delta^{18}O$ value of +6.62‰ for blue- and red-luminescent, corroded-appearing grain cores. Grains are zoned first to a bright-green zone with $\delta^{18}O$ of +4.45‰ and then dark-green luminescent zones $\delta^{18}O$ of +6.22‰ (Figs. 2 and 7). Burmese jadeitite sample CJ-01, a river cobble from the conglomerate jade mining area of Nansibon, has blue-luminescent zones with $\delta^{18}O$ values of +8.89 to 9.33‰, and yellow-green-luminescent zones with $\delta^{18}O$ values of +4.90

to 6.94‰. Jadeitites thus may show little zoning of $\delta^{18}O$ with respect to CL, or display bright-green to yellow-green CL zones with either heavier (112538) or lighter (112552-1; CJ-01) $\delta^{18}O$ values than red-, blue-, or dark-green-luminescent zones in the same samples or grains.

Discussion

Temperature of equilibration of jadeite and albite

Samples 112538 and CJ-01 contain adjacent grains of jadeite and albite. This permits the application of the jadeite-albite oxygen-isotope thermometer calibrated by Matthews et al. (1983, 1994) and Zheng (1993). The calibration equations are extended by ~200 °C below the calibration conditions for jadeite-water, and 100 °C below those for albite-water. It is perhaps not surprising that sample CJ-01 yields *T*-estimates ranging from ~173 to 257 °C, and sample 112538 from –30 to 67 °C (Table 5). The latter sample is from a jadeitite-albitite rock in which textures such as broken zoned jadeite crystals healed by albite indicate that albite postdates jadeite and may not be in equilibrium with it. These *T*-estimates support a lack of equilibrium between jadeite and albite in sample 112538. That disequilibrium is the case for 112538 is borne out by the low- to below-zero-degree temperature estimates obtained by matching the blue-jadeite-armored, yellow-luminescent cores of CJ-01 grains with albite $\delta^{18}O$ values for that sample. These pairs are texturally not in equilibrium, and yield impossibly low temperature estimates.

The 257 °C estimate for sample CJ-01 does not agree well with the oxygen-isotope-based temperature estimate of 401 °C made for a jadeite-albite pair from a Guatemalan jadeitite sample (Johnson and Harlow 1999). However, those authors also

Table 5. Jadeite-albite geothemometry

Albite	$\delta^{18}O$	Jadeite	$\delta^{18}O$	α	1000ln(α)	Matthews et al. 1983 *T*, °C	Matthews 1994 *T*, °C	Zheng 1993 *T*, °C
112538	12.3	112538 Red CL	4.6	1.007624622	7.595701239	6	41	–54
	12.3	112538 Blue CL	4.9	1.007343868	7.317033270	11	47	–48
"co-existing"*	12.3	112538 Green CL	5.7	1.006522561	6.501380653	28	67	–30
CJ-01	11.9	CJ-01 Yellow 1 CL	4.9	1.006965867	6.941717681	19	56	–40
	11.9	CJ-01 Yellow 2 CL	6.4	1.005485006	5.470017801	55	97	0
	11.9	CJ-01 Yellow 3 CL	6.9	1.004925815	4.913722712	74	118	21
	11.9	CJ-01 Blue 1 CL	8.9	1.002983477	2.979035156	172	229	141
	11.9	CJ-01 Blue 2 CL	9.3	1.002546244	2.543007362	209	270	189
"co-existing"*	11.9	CJ-01 Blue 3 CL	9.2	1.002675386	2.671813969	197	257	173

* "co-existing" = based on grain-grain contacts. See text for explanation.

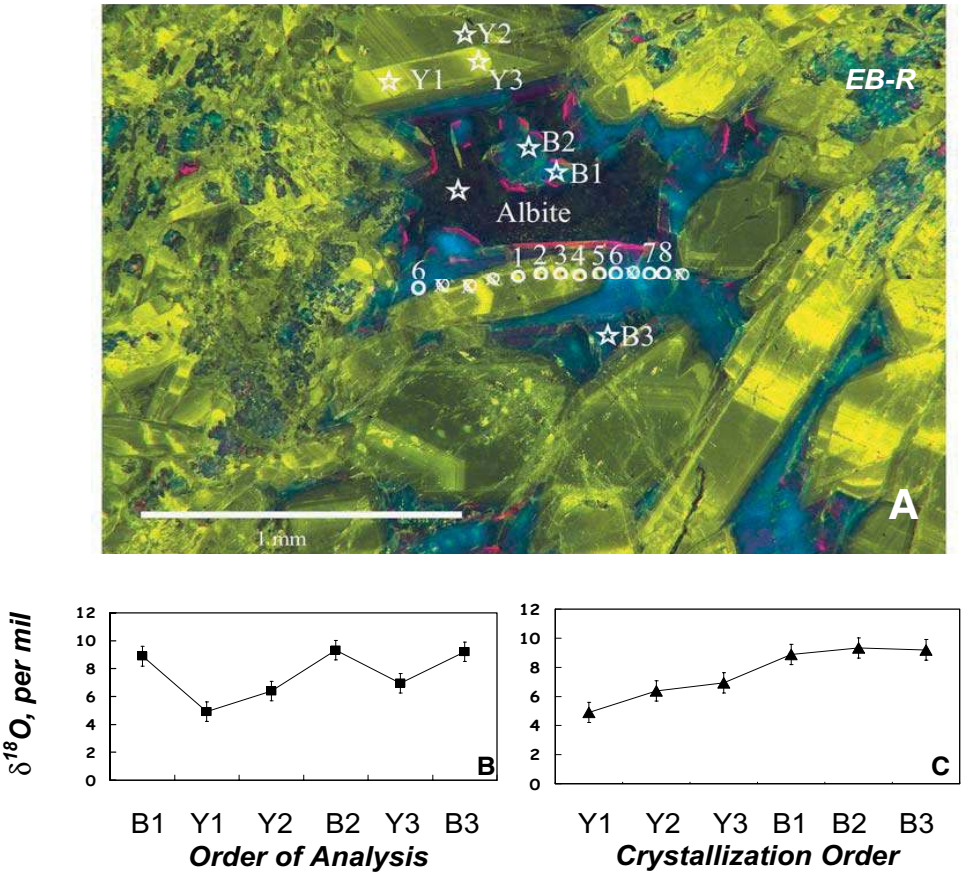

Figure 8. CL image with ion-microprobe craters (**a**) and $\delta^{18}O$ values (**b** and **c**) for sample CJ-01. The scale bar in the lower left corner of **a** is 1 mm long. The circles numbered 1–8 mark craters of sites analyzed for trace elements, whereas stars labeled "Y1-3," "B1-3," and "Albite" show sites analyzed for oxygen isotopes. Symbol sizes represent the size of the craters produced by the O or Cs ion beams, and thus the region analyzed. This image was obtained after the C-coat used for trace-element analysis was removed, but prior to additional polishing and Au-coating of the sample for oxygen-isotope analysis. The isotope analysis sites were mapped on to the diagram after most of the Au-coat was removed. The abbreviation "EB-R" in **a** indicates a patchy, partly consumed-appearing, blue- and red-luminescent, "early" core of jadeite that is overgrown by yellow-green jadeite (see text).

obtained an entrapment temperature of 272 °C for primary fluid inclusions, a value near the maximum-*T* estimate for CJ-01. Furthermore, phase-equilibrium-based estimates of *T* conditions of Guatemalan jadeitites range from 200 to 400 °C (Harlow 1994). Thus, it is possible that the new estimate for sample CJ-01 is credible, and that this is merely another example of a very low-*T* jadeitite. Alternatively, either the calibration equations have been overextended, or the albite and jadeite are not in equilibrium, as seems likely for sample 112538.

Integrated geochemical variations and textural development, sample CJ-01

The relative abundances of diverse geochemical groups of trace elements and the values of $\delta^{18}O$ all vary systematically and widely through the growth history of jadeite grains in sample CJ-01 (Table 3, Figs. 6 and 8). The CL microstructures indicate that red- and blue-luminescent jadeite crystallized first; this is seen in the ragged patches of such jadeite in grain cores (for example, "EB-R" in Fig. 8). Subsequent to its crystallization, the early jadeite was resorbed or partly consumed. It is not possible to see from the remnants whether early grains were idioblastic in their CL zoning. The early, blue- and red-luminescent jadeite was overgrown by yellow-green-luminescent jadeite, which displays prominent idioblastic, oscillatory zoning features, marked by changes of CL brightness. Finally, the oscillatory zoned, yellow-green-luminescent jadeite was overgrown by blue-, then red-luminescent jadeite. What appear to have been fluid-filled spaces are occupied by non-luminescent albite.

Cloos (1986) interpreted the idioblastic growth of high-*P* minerals into what now appear to be vugs within Franciscan eclogite to reflect that the empty space was, at high-*P* conditions, filled with fluid, and therefore fluid pressure was equal to lithostatic pressure. An analogous interpretation for jadeitite seems inevitable: fluids evidently occupied mm-scale pores in the jadeitites during some episodes of jadeite crystallization. Because the earliest jadeite generation in sample CJ-01 is resorbed and was partly consumed, it seems likely that the fluid, which precipitated the yellow-green-luminescent, more diopsidic jadeite around the red and blue remnants, was the agent of dissolution, and that that fluid was not in equilibrium with the composition of the first generation of jadeite. In contrast, the blue-to-red-zoned rims on this yellow-green-luminescent jadeite do not appear to have corroded the latter, so it is possible that the second zone of blue-luminescent jadeite was in equilibrium at its interface with the yellow-CL jadeite it surrounds.

The abundance data for trace elements show great changes in Rb, Ti, Cr, Sr, Zr, and Hf contents during the crystallization interval of yellow-green-luminescent, oscillatory-zoned jadeite (Figs. 6 and 8). However, the interpretation of these changes is hampered by lack of an absolute chronometer. In the case of Rb and Cr, elemental abundances appear to have increased throughout the crystallization interval of yellow-green luminescent jadeite, and then sharply decreased as blue-luminescent jadeite began to crystallize. Strontium, Er, and Y abundances "peaked" within the crystallization interval of yellow-green-luminescent jadeite, and continued to drop as blue-luminescent jadeite grew. Both Zr and Hf decreased throughout grain growth. Lithium and Sm showed nearly constant values through the crystallization of yellow-green-luminescent jadeite, then dropped to much lower values as blue-luminescent jadeite began to grow.

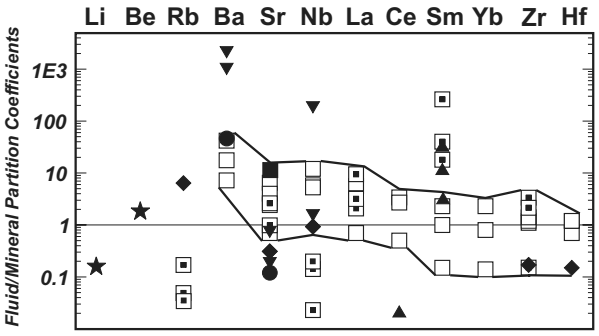

FIGURE 9. Compilation of fluid-clinopyroxene partition coefficients. Symbols indicate data sources, as follows: filled stars, Brenan et al. (1998); filled diamonds, Adam et al. (1997); filled circles, Keppler (1996); filled squares, Najorka et al. (1999); open squares, Stalder et al. (1998); center-filled squares, Ayers et al. (1997); downward-pointing triangles, Brenan et al. (1995); and upward-pointing triangles, Mysen (1979).

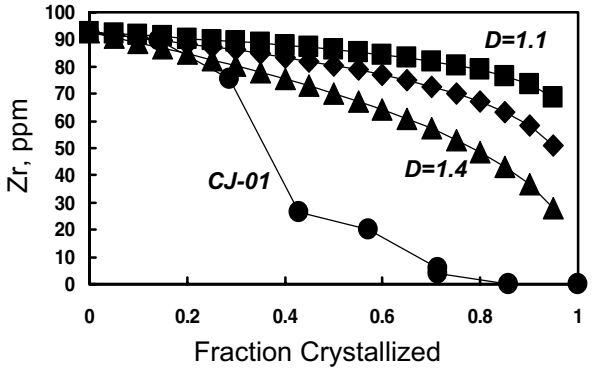

FIGURE 10. Closed-system fractional crystallization models for Zr in sample CJ-01. A range of fluid-clinopyroxene partition coefficients from 1.1 to 1.4 encompasses all but two of the published data shown in Figure 9. To compare the SIMS data with these calculated curves, analysis points for the grain analyzed from sample CJ-01 were arbitrarily apportioned evenly along the X-axis, which is labeled as "fraction crystallized" (see text). Models were calculated based on the equation given by Haskin (1984). See text for discussion.

CJ-01 jadeite lacks evidence for closed-system fractional crystallization with respect to Zr. Although the reasoning that follows cannot be applied to every trace element in these grains for lack of data, a range of fluid-mineral partition coefficients (*D*-values) exists for Zr in omphacitic clinopyroxene, which is similar enough to jadeite—and particularly to relatively Ca-rich jadeite—that calculations of the amount and fractionation of Zr in jadeite probably can be compared with the actual Zr abundances measured in a zoned grain. Figure 9 shows a compilation of the fluid-omphacite *D*-values for a variety of elements from literature sources, and Figure 10 illustrates the comparison of Zr contents of a clinopyroxene derived from fractional crystallization calculations with the zoning pattern of Zr in CJ-01 jadeite. No matter which value for the fluid-omphacite partition coefficient

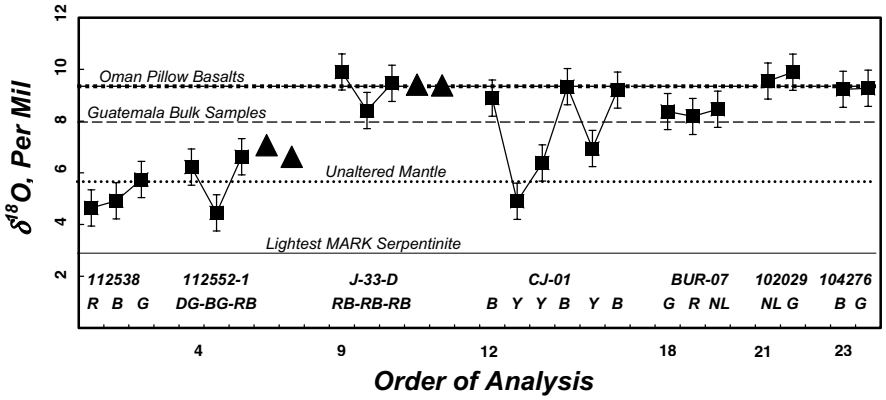

FIGURE 11. Comparison of $\delta^{18}O$ values for jadeite with subduction-zone components. Lines are as follows: heavy dotted line, value for Oman pillow basalts (Gregory and Taylor 1981); range between the Oman pillow basalt line and the dashed line, values obtained for Guatemalan jadeitites (Johnson and Harlow 1999); light dotted line, unaltered mantle (Taylor 1968; Gregory and Taylor 1981); and light solid line, lightest MARK serpentinite (Haggerty 1991). Abbreviations for CL colors are as in Figure 7.

for Zr is selected, the fractional crystallization models all predict smooth decreases of Zr contents in pyroxene, from small to large degrees of crystallization. Although Zr decreases rimward in the grain, CJ-01 clinopyroxene also records an abrupt large decrease in Zr, which correlates with the change from yellow-green to blue-luminescent jadeite. These features cannot be reconciled with fractional crystallization alone, and suggests the system was open when the second generation of blue-red luminescent jadeite crystallized.

In contrast to the trace-element abundances, which generally decrease during the crystallization of CJ-01 jadeite (Table 3, Figs. 6e and 10), $\delta^{18}O$ values increase from the interior to the exterior of grains, from +4.9 to 9.3‰ (Table 4, Fig. 8c). An increase of +6.9 to 8.9‰ occurs between the outer yellow-green-luminescent zone and the inner blue-luminescent overgrowth. The other two values for blue-luminescent jadeite are only ~0.4‰ greater, or within analytical error. It appears that the fluid from which blue-luminescent jadeite crystallized is distinct in both its trace-element signature and oxygen-isotope composition from that which deposited the yellow-green luminescent jadeite.

Possible sources of jadeitite forming fluids

The jadeitite oxygen-isotope data resemble other studies of oxygen isotopes in subduction-zone metamorphic rocks. Johnson and Harlow (1999) analyzed mineral separates from Guatemalan jadeitites. Seven samples of jadeite mineral separates yielded $\delta^{18}O$ values of +8.0 to 9.4‰, within the range of 15 of the 26 analyses of this study, including the two jadeitite separates from sample J-33-D analyzed by laser fluorination (Fig. 11). The $\delta^{18}O$ values of Johnson and Harlow (1999) are heavier than fluids in equilibrium with unaltered oceanic crust and mantle, because the average value for MORB and oceanic peridotite is 5.8 ± 0.3‰ (e.g., Taylor 1968; Muehlenbachs and Clayton 1972; Kyser et al. 1982). Johnson and Harlow (1999) interpreted this to reflect jadeitite formation from serpentinizing fluids at depth within a subduction zone. In contrast, the sample from Guatemala analyzed in this study, NMNH 112538, displays the lightest average $\delta^{18}O$ from + 4.7 to 5.7‰ (Table 4). The Guatemala jadeitites may thus show evidence for heterogeneous fluid equilibration, of the type documented for metagabbros and metamorphosed pillow basalts in other subduction complexes (e.g., Miller and Cartwright 2000; Putlitz et al. 2000; Frueh-Green et al. 2001; Miller et al. 2001).

Miller and Cartwright (2000) compared oxygen-isotope values from variably metamorphosed pillow basalts from Alpine Corsica (France), the Ligurian ophiolite (Italy), and the Zermatt-Sass ophiolite zone (Switzerland). Rocks from two areas unaffected by high-pressure metamorphism also were studied. The authors sampled cores and rims of pillows. Rocks affected by high-pressure metamorphism displayed cores heavier in $\delta^{18}O$ than rims, the opposite of rocks that were unmetamorphosed or incipiently metamorphosed. The latter two rock types and most of the lower *T*, high-*P* metamorphosed rocks display $\delta^{18}O$ values significantly heavier than igneous ones. This indicates that most of the suites had been altered by fluid-rock interaction, most likely on the seafloor. Because the cores of high-*P* pillows are heavier in $\delta^{18}O$ values than rims, there was likely some fluid-rock interaction during subduction with a fluid that was lighter than those of the pillow lavas. The authors suggested such a fluid might be derived from deeper within the stratigraphy of the subducting ophiolite.

Putlitz et al. (2000) analyzed oxygen isotopes in eclogite-facies metagabbros and metabasalts from the Cycladic archipelago (Greece). Those authors analyzed mineral separates and whole rock samples of metagabbros, and calculated whole-rock compositions based on mineral separate analyses of the metabasalts. The study included both Fe- and Mg-rich metagabbros, which the authors interpreted to represent two different types of magma-chamber-related, oceanic crust. Previous studies of the phase assemblages indicate $P > 14$ kbar, $T = 500 \pm 30$ °C. The range of whole-rock metagabbro $\delta^{18}O$ values is +3.44 to 6.45‰, and the estimated whole-rock values for metabasalts are +9.9 to 11.3‰. The authors reported a clear offset between the $\delta^{18}O$ values of garnet, omphacite, and glaucophane from metagabbros (+2.6 to 7.1‰) vs. metabasalts (+9.4 to 12.6‰). The metagabbro data are thought to reflect both pristine igneous values and evidence for high-*T* hydrothermal alteration (of ocean floor origin) in the

lighter values. The metabasalt data are interpreted to show evidence for alteration in the presence of seawater at temperatures below ~300 °C. As in the case of the Miller and Cartwright (2000) study, the evidence for two types of isotopic signatures was interpreted to record alteration of oceanic slab rocks prior to subduction.

Frueh-Green et al. (2001) examined the isotopic systematics of high-pressure ultramafic rocks and eclogitic metagabbros of the Erro-Tobbio peridotite (western Italian Alps). These authors obtained data for relatively undeformed and mylonitic metaultramafic rocks, and for eclogitic metagabbros. Serpentinized mantle peridotites showed whole-rock $\delta^{18}O$ values between +5.7 and 8.1‰. Relatively undeformed (but metamorphosed) ultramafic rocks yielded whole-rock $\delta^{18}O$ values between +4.9 and 7.6‰, high-pressure metamorphosed serpentinite mylonites values of +5.3 to 6.7‰, and eclogitic metagabbros values of +3.1 to 5.3‰. The authors interpreted their oxygen-isotope data to testify to both high- (>300 °C) and low-*T* fluid-rock interaction. Rocks with $\delta^{18}O$ values <5‰ were interpreted to have been altered at high-*T* conditions in sea-floor hydrothermal systems prior to subduction. Those with $\delta^{18}O$ values >>5.8‰ were interpreted to show evidence for low-*T* hydration on the sea floor, preserved into the eclogite facies.

Miller et al. (2001) analyzed an oxygen-isotope profile through the H*P*-L*T* ophiolitic rocks of Corsica, though a metamorphic gradient from prehnite-pumpellyite to lawsonite-eclogite facies, in ophiolitic rock types from pillow basalt to serpentinite and serpentinized peridotite. Those authors found an overall decrease from whole-rock $\delta^{18}O$ values between +11.6 to 14.6‰ for pillow breccia samples, to whole-rock ranges of +3.6 to 6.7‰ for serpentinites and peridotites. The whole-rock $\delta^{18}O$ values of pillow basalt samples ranged from +6.4 to 13.8‰, and "metabasalts" from +6.0 to 15.6‰. Overall, they noted the decrease with depth in the ophiolite stratigraphy that is also seen in on-land ophiolites. In the latter terrains, this feature is interpreted to reflect seafloor hydrothermal systems. The preservation of such a signature in the Corsican metaophiolite was thought to reflect a lack of both large-scale, pervasive fluid flow and/or incursion of exotic fluid during the metamorphism of this terrain.

Under different conditions, these terrains, which show little evidence for large-scale fluid flow during high-*P* metamorphism, all could be possible sources of jadeitite-forming subduction-zone fluids. This is because they contain rocks that had undergone both low- and high-*T* alteration on the sea floor, prior to subduction. The oxygen isotope study of Johnson and Harlow (1999) on bulk mineral separates from Guatemala shows evidence of jadeitite formation from a low-*T*, slightly heavy oxygen source, which is one of the types of fluids that could be derived from such terranes. A major difference between the Alpine-Cycladean and jadeitite-bearing terrains, of course, is that the latter show evidence for the introduction of significant amounts of fluid to the serpentinite-matrix mélanges in which jadeitite occurs (Johnson and Harlow 1999; Harlow and Sorensen 2005). However, Miller et al. (2001) pointed out that terrains with evidence for large-scale fluid flow, such as the Catalina Schist, show strong evidence for focusing of such fluid flow in mélange zones. Furthermore, those authors stated that zones of channelized fluid-flow might be difficult to detect in terrains that lack such obvious features as much hybridized mélanges. Nonetheless, Alpine-Cycladean types of terrains show that a wide range of $\delta^{18}O$ values are present in subducted oceanic crust, and that devolatilization of such crust could yield a wide range of $\delta^{18}O$ in fluid compositions.

What combinations of sources and mechanisms could produce fluids that would particularly favor the crystallization of jadeitite? First, a source for Na is needed. Potential Na reservoirs in subducted zones include: seawater; albite-consuming reactions involving spilitized ocean floor basalt; Si-poor, fluid-dominated systems that pass through and equilibrate with spilite; and low (~1–5%) chlorinity aqueous fluids generated by the devolatilization of blueschist to eclogite (Manning 1998). Manning (1998) determined that, for fluids with 0.001 to 1.0 molal Cl, at temperatures of 500 to 600 °C and pressures of 15 to 20 kb, the relative solubilities are: Si ~Na >Al > Mg. with quartz at or near saturation. Manning (2004) notes that such fluids are likely expressed as veining by sodic minerals in blueschists and eclogites, and furthermore that aqueous fluid in equilibrium with jadeite-peridotite is Si- and Na-rich, with substantial Al. If such fluids were able to migrate to shallower, cooler conditions without crystallizing all of their solute load, might they also be capable of producing jadeite veins in serpentinizing peridotite?

Most of the pore seawater that is initially subducted is likely removed at depths shallower than those of jadeitite crystallization (~8 to 12 kbar: Harlow and Sorensen 2005; Harlow 1994). However, Giaramita and Sorensen (1994) reported primary fluid inclusions with seawater equivalent salinities from clinopyroxene in eclogite blocks from the Dominican Republic, for which they estimated P_{min} ~10 kbar and T ~550 °C. This is evidence that at least aqueous fluid of approximately seawater salinity is present under eclogite-facies conditions. Spilitized ocean floor basalts contain larger amounts of Na_2O than their protoliths (e.g., Melson and Van Andel 1968), mostly as albite. Taken together, these data at least raise the possibility that blueschists derived from such spilitized protoliths might have both mildly saline fluids trapped in their minerals and Na-rich compositions. If such blueschists were to devolatilize, they might yield fluids that could crystallize jadeitite.

Experiments have suggested that both LILE and LREE can migrate through serpentine in aqueous fluids, without significantly interacting with the rock (e.g., Tatsumi and Eggins 1995). These observations are pertinent to both the existence of jadeitites, which show textural evidence for having crystallized from a fluid that contained Na, Al, and Si, and evidence for the complex trace-element zoning within constitutent jadeite grains. The complex chemical zoning of such jadeite, along with the overall geochemical evolution of jadeitite, may uniquely record the migration of certain types of slab-derived fluids through overlying ultramafic rocks.

This study also indicates that the compositions of jadeite grains probably mirror those of the fluids from which they grew. The different-colored CL zones in each sample, and their various trace-element and oxygen-isotope compositions, suggest several things about parental fluids. Three types of fluid formed worldwide jadeitite deposits: one derived from rocks that had previously been altered by seawater at T < 300 °C ("seafloor weathering"); another from rocks previously altered in a high-*T* sea floor hydrothermal system; and a third in equilibrium with

an "igneous" or "mantle" source. The first jadeite precipitated directly from a relatively trace-element-poor fluid in a serpentinite host within an active subduction zone. Later, additional jadeite crystallized as this fluid mixed (to varying degrees) with locally derived, serpentinizing fluids. Both stages took place within an active subduction zone. This scenario is guided by the textural and geochemical observations that the first jadeite to crystallize in a given cycle is blue- or red-luminescent, trace-element poor, and very near the jadeite end-member in composition, whereas later stages of grain growth in a cycle are yellow-green luminescent, trace-element-(especially REE-) rich, and contain up to 10% of diopside substitution. The highly valued "imperial green" veinlets and patches within jadeitites are Cr-rich; textures indicate these form during the latest stages of crystallization of a given jadeitite block, and may represent exchange or enrichment of jadeitite-forming fluids and local serpentinizing ones. The scale of movement of jadeitite-forming fluids is as yet unknown, because jadeitite occurs in serpentinite-matrix mélanges along with lawsonite eclogite, eclogite, garnet blueschist, garnet amphibolite, and other high *P*/*T* rock types. Jadeitite likely represents an important, if rarely observed, variety of subduction-zone fluid, fortuitously preserved in a beautiful and highly valued gemstone.

ACKNOWLEDGMENTS

This paper was reviewed by Mark Cloos and Jodie Miller, and we thank them very much for their thoughtful and detailed comments. The thorough and patient editing of William D. Carlson is greatly appreciated. S.S.S. thanks the Sprague Fund of the Smithsonian Institution for seven years of support for this project, and SSS and GEH thank recent support from NSF through grant EAR-0309320. Support for laser-fluorination oxygen-isotope analyses was provided by the US National Science Foundation, Continental Dynamics program, EAR-0003276 (Rumble). We thank James Rougvie of Beloit College for performing the fractionation calculations while a DOE-funded Smithsonian Institution postdoctoral fellow with SSS. We appreciate discussions with Virginia B. Sisson and Hans Avé Lallemant. We also acknowledge the influence of the late Hatten S. Yoder in this work, both through the original Yoder and Chesterman (1951) collection, now in the Smithsonian (and to which sample J-33-D belongs) and to Hat's interest in the CL of jadeitites. Many thanks also to Erik Hauri and Jianhua Wang, Department of Terrestrial Magnetism, Carnegie Institution of Washington, for running the Cameca 6F ion microprobe and training S.S.S. as a user. Finally, this paper owes a deep debt to the work of Wallace Gary Ernst, who has taught us and many others so much about subduction-zone processes during his more than 40 years of research at UCLA and Stanford University. Gary has studied many jadeite-bearing rocks, although he has yet to venture into the Burmese or Guatemalan jade fields. We dedicate this paper to Gary to honor his official retirement from Stanford University, which took place in June, 2004. About these data, we quote one of Gary's favorite observations: "Anything that did happen, can happen." May this installment of the jadeitite story be a suitable gift to the master translator of subduction-zone tales.

REFERENCES CITED

Adam, J., Green, T.H., Sie, S.H., and Ryan, C.G. (1997) Trace element partitioning between aqueous fluids, silicate melts, and minerals. European Journal of Mineralogy, 9, 569–584.

Ayers, J.C., Dittmer, S.K., and Layne, G.D. (1997) Partitioning of elements between peridotite and H_2O at 2.0–3.0 GPa and 900–1100 °C, and applications to models of subduction zone processes. Earth and Planetary Sciences Letters, 150, 381–398.

Bebout, G.E. (1996) Volatile transfer and recycling at convergent margins: mass-balance and insights from high-*P*/*T* metamorphic rocks. In G.E. Bebout, D.W. Scholl, S.H. Kirby, and J.P. Platt, Eds., Subduction Top to Bottom, 96, 179–193. Geophysical Monograph, American Geophysical Union, Washington, D.C.

Bebout, G.E. and Barton, M.D. (1989) Fluid flow and metasomatism in a subduction-zone hydrothermal system: Catalina Schist terrane, California. Geology, 17, 976–980.

——— (1993) Metasomatism during subduction: products and possible paths in the Catalina Schist, California. Chemical Geology, 108, 61–92.

Bebout, G.E., Ryan, J.G., Leeman, W.P., and Bebout, A.E. (1999) Fractionation of trace elements by subduction-zone metamorphism-effect of convergent margin thermal evolution. Earth and Planetary Science Letters, 171, 63–81.

Berger, G., Schott, J., and Guy, C. (1988) Behavior of Li, Rb, and Cs during basalt glass and olivine dissolution and chlorite, smectite, and zeolite precipitation from seawater: Experimental investigations and modeling between 50 and 300 °C. Chemical Geology, 71, 297–312.

Bishop, R.L., Lange, F.W., and Easby, E.K. (1991) Jade in Mesoamerica: Pre-Columbian Jade in the Central and Southern Americas. In R. Keverne, Ed., Jade, 316–341. Anness Publishing, London.

Bishop, R.L., Sayre, E.V., and Mishara, J. (1993) Compositional and structural characterization of Maya and Costa Rican jadeitites. In F.W. Lange, Ed., Pre-columbian Jade, a Proceedings Volume from a Conference on Middle American Jade, p. 30–60. University of Utah Press, Salt Lake City, Utah.

Brenan, J.M., Shaw, H.F., Ryerson, F.J., and Phinney, D.L. (1995) Mineral-aqueous fluid partitioning of trace elements at 900 °C and 2.0 GPa; constraints on the trace element chemistry of mantle and deep crustal fluids. Geochimica et Cosmochimica Acta, 59, 3331–3350.

Brenan, J.M., Ryerson, F.J., and Shaw, H.F. (1998) The role of aqueous fluids in the slab-to-mantle transfer of boron, beryllium and lithium during subduction: experiments and models. Geochimica et Cosmochimica Acta, 62, 3337–3347.

Catlos, E.J. and Sorensen, S.S. (2003) Phengite-based Chronology of K- and Ba-rich Fluid Flow in Two Paleosubduction Zones. Science, 299, 92–95.

Chan, L.H., Leeman, W.P., and You, C.-F. (1999) Lithium isotopic composition of Central American volcanic arc lavas: Implications for modification of subarc mantle by slab-derived fluids. Chemical Geology, 160, 255–280.

Chhibber, H.L. (1934) The Mineral Resources of Burma, 309 p. MacMillan and Co., Ltd., London.

Chihara, K. (1971) The mineralogy and petrology of jadeites from the Omi-Kataki area, Central Japan. Mineralogical Society of Japan, Special Paper, 147–156.

Class, C., Miller, D.M., Goldstein, S.L., and Langmuir, C.H. (2000) Distinguishing melt and fluid subduction components in Umnak volcanics, Aleutian arc. Geochemistry Geophysics Geosystems, 1, Art. No. 1999GC000010.

Cloos, M. (1986) Blueschists in the Franciscan subduction complex of California: Petrotectonic constraints on uplift mechanisms. Geological Society of America Memoir, 164, 77–94.

Dobretsov, N.L. (1984) The jadeite and problem of ophiolites (in Russian). Geologiya I Geofizika, 12, 80–88.

Domanik, K.J., Hervig, R.L., and Peacock, S.M. (1993) Beryllium and boron in subduction zone minerals: An ion microprobe study. Geochimica et Cosmochimica Acta, 57, 4997–5010.

Eiler, J.M., Graham, C.M., and Valley, J.W. (1997) SIMS analysis of oxygen isotopes; matrix effects in complex minerals and glasses. Chemical Geology, 138, 221–244.

Elliott, T., Jeffcoate, A., and Bouman, C. (2004) The terrestrial Li isotope cycle: light-weight constraints on mantle convection. Earth and Planetary Science Letters, 220, 231–245.

Foshag, W.F. (1957) Mineralogical studies on Guatemalan jade. Smithsonian Miscellaneous Collections 135, 5, 60 p.

Frueh-Green, G., Scambelluri, M., and Vallis, F. (2001) O-H isotope ratios of high pressure ultramafic rocks: implications for fluid sources and mobility in the subducted hydrous mantle. Contributions to Mineralogy and Petrology, 141, 145–159.

Giaramita, M.J. and Sorensen, S.S. (1994) Primary fluids in low temperature eclogites: evidence from two subduction complexes Dominican Republic and California, U.S.A. Contributions to Mineralogy and Petrology, 117, 279–292.

Gregory, R.T. and Taylor, H.P. (1981) An oxygen isotope profile in a section of Cretaceous oceanic crust, Samail ophiolite, Oman: evidence for $\delta^{18}O$ buffering of oceans by deep (>5 km) seawater-hydrothermal circulation at mid-ocean ridges. Journal of Geophysical Research, 86, 2737–2755.

Haggerty, J.A. (1991) Evidence from fluid seeps atop serpentine seamounts in the Mariana Forearc: Clues for emplacement of the seamounts and their relationship to forearc tectonics. Marine Geology, 102, 293–309.

Harlow, G.E. (1993) Middle American jade: geologic and petrologic perspectives on its variability and source. In F.W. Lange, Ed., Precolumbian Jade, a Proceedings volume from a Conference on Middle American Jade, p. 9–29. University of Utah Press, Salt Lake City, Utah.

——— (1994) Jadeitites, albitites, and related rocks from the Motagua Fault Zone, Guatemala. Journal of Metamorphic Geology, 12, 49–68.

Harlow, G.E. and Sorensen, S.S. (2001) Jade: Occurrence and metasomatic origin. Australian Gemmologist, 21, 7–10.

——— (2005) Jade (nephrite and jadeitite) and serpentinite: Metasomatic connections. International Geology Review, 47, 113–146.

Harlow, G.E., Sisson, V.B., Avé Lallemant, H.G., and Sorensen, S.S. (2003) High-pressure metasomatic rocks along the Motagua Fault Zone, Guatemala. Ofioliti, 28, 115–120.

Haskin, L.A. (1984) Petrogenetic modeling—use of rare earth elements. In P. Henderson, Ed., Rare Earth Element Geochemistry, Developments in Geochemistry, 2, 115–152. Elsevier, Amsterdam.

Hughes, R.W., Galibert, O., Bosshart, G., Ward, F., Thet, O., Smith, M., Sun,

T.T., and Harlow, G.E. (2000) Burmese Jade: The Inscrutable Gem. Gems and Gemology, 36, 2–26.
Jarosewich, E., Nelen, J.A., and Norberg, J.A. (1980) Reference samples for electron microprobe analysis. Geostandards Newsletter, 4, 43–47.
Johnson, C.A. and Harlow, G.E. (1999) Guatemala jadeitites and albites were formed by deuterium-rich serpentinizing fluids deep within a subduction zone. Geology, 27, 629–632.
Keppler, H. (1996) Constraints from partitioning experiments on the composition of subduction-zone fluids. Nature, 380, 237–240.
Kyser, T.K., O'Neil, J.R., and Carmichael, I.S.E. (1982) Genetic relations among basic lavas and ultramafic nodules: Evidence from oxygen isotope compositions. Contributions to Mineralogy and Petrology, 81, 88–102.
Lasnier, B., Poirot, J.-P., and Smith, D.C. (1992) Intercroissances de jadeite de differentes compositions dans jades revelés par cathodoluminescence. Revue de Gemmologie A.F.G., 113, 8–11.
Leeman, W.P. (1996) Boron and other fluid-mobile elements in volcanic arc lavas: Implications for subduction processes. In G.E. Bebout, D. Scholl, S. Kirby, and J.P. Platt, Eds., Subduction Top to Bottom, 96, p. 269–276. Geophysical Monograph, American Geophysical Union, Washington, D.C.
Manning, C.E. (1998) Fluid composition at the blueschist-eclogite transition in the model system Na2O-MgO-Al2O3-SiO2-H2O-HCl. Swiss Bulletin of Mineralogy and Petrology, 78, 225–242.
——— (2004) The chemistry of subduction zone fluids. Earth and Planetary Science Letters, 223, 1–16.
Marshall, D.J. (1988) Cathodoluminescence of geological materials, 146 p. Unwin Hyman, Boston.
Matthews, A. (1994) Oxygen isotope geothermometers for metamorphic rocks. Journal of Metamorphic Geology, 12, 211–219.
Matthews, A., Goldsmith, J.R., and Clayton, R.N. (1983) Oxygen isotope fractionations involving pyroxenes: the calibration of mineral-pair thermometers. Geochimica et Cosmochimica Acta, 47, 631–644.
Miller, J.A. and Cartwright, I. (2000) Distinguishing between seafloor alteration and fluid flow during subduction using stable isotope geochemistry: examples from Tethyan ophiolites in the western Alps. Journal of Metamorphic Geology, 18, 467–482.
Miller, J.A., Cartwright, I., Buick, I.S., and Barnicoat, A. (2001) An O-isotopic profile through the H*P*-L*T* Corsican ophiolite, France and its implications for fluid flow during subduction. Chemical Geology, 178, 43–69.
Miller, J.A., Buick, I.S., Cartwright, I., and Barnicoat, A. (2002) Fluid processes during the exhumation of high-*P* metamorphic rocks. Mineralogical Magazine, 66, 93–119.
Moran, A.E., Sisson, V.B., and Leeman, W.P. (1992) Boron in subducted oceanic crust and sediments: effects of metamorphism and implications for arc magma compositions. Earth and Planetary Science Letters, 111, 331–349.
Morris, J.D., Leeman, W.P., and Tera, F. (1990) The subducted component in island arc lavas; constraints from B-Beisotopes and Be systematics. Nature, 344, 6261, 31–36.
Muehlenbachs, K. and Clayton, R.N. (1972) Oxygen isotope studies of fresh and weathered submarine basalts. Canadian Journal of Earth Sciences, 9, 172–184.
Mysen, B. (1979) Trace element partitioning between garnet peridotite minerals and water-rich vapor; experimental data from 5 to 30 kbar. American Mineralogist, 64, 274–287.
Najorka, J., Gottschalk, M., Franz, G, and Heinrich, W. (1999) Ca-Sr distribution among amphibole, clinopyroxene, and chloride-bearing solutions. American Mineralogist, 84, 596–606.
Pagel, M., Barbin, V., Blanc, P., and Ohnenstetter, D., Eds. (2000) Cathodoluminesence in Geosciences, 514 p. Springer, Berlin.
Peacock, S.M. (1990) Fluid processes in subduction zones. Science, 248, 329–337.
——— (1991) Numerical simulation of subduction zone pressure-temperature-time paths: Constraints on fluid production and arc magmatism. Philosophical Transactions of the Royal Society, London, Series A, 335, 341–353.
——— (1993a) The importance of blueschist → eclogite dehydration reactions in subducting oceanic crust. Geological Society of America Bulletin, 105, 684–694.
——— (1993b) Large-scale hydration of the lithosphere above subducting slabs. Chemical Geology, 108, 49–59.
Ponalho, J. (1986) Quantitative cathodoluminescence; a modern approach to gemstone recognition. Journal of Gemmology, 21, 182–193.
——— (1999) Cathodoluminescence du jade. Revue de Gemmologie, 137, 10–16.
——— (2000) Cathodoluminesence as a tool in gemstone identification. In M. Pagel, V. Barbin, P. Blanc, and D. Ohnenstetter, Eds., Cathodoluminesence in Geosciences, p. 479–500. Springer, Berlin.
——— (2002) Inclusions in gemstones; their cathodoluminescence (CL) and CL spectra. Journal of Gemmology, 28, 85–100.
Putlitz, B., Matthews, A. and Valley, J.W. (2000) Oxygen and hydrogen isotope study of high pressure metagabbros and metabasalts (Cyclades, Greece): implications for the subduction of oceanic crust. Contributions to Mineralogy and Petrology, 138, 114–126.
Ryan, J., Morris, J., Bebout, G., and Leeman, B. (1996) Describing chemical fluxes in subduction zones: insights from "depth-profiling" studies of arc and forearc rocks. In G.E. Bebout, D. Scholl, S. Kirby, and J.P. Platt, Eds., Subduction Top to Bottom, 96, p. 263–268. Geophysical Monograph, American Geophysical Union, Washington, D.C.
Schmidt, M.W. and Poli, S. (1998) Experimentally based water budgets for dehydrating slabs and consequences for arc magma generation. Earth and Planetary Science Letters, 163, 361–379.
Seyfried, W.E., Jr., Chen, X., and Chan, L.-H. (1998) Trace element mobility and lithium isotope exchange during hydrothermal alteration of seafloor weathered basalt: An experimental study at 350 °C, 500 bar. Geochimica et Cosmochimica Acta, 62, 949–960.
Shi, G.H., Cui, W.Y., Wang, C.Q., and Zhang, W.H. (2000) The fluid inclusions in jadeitite from Pharkant area, Myanmar. Chinese Science Bulletin, 45, 1896–1900.
Shi, G.H., Cui, W.Y., Tropper, P., Wang, C.-Q., Shu, G.M., and Yu, H. (2003) The petrology of a complex sodic and sodic-calcic amphibole association and its implications for the metasomatic processes in the jadeitite area in Northwestern Myanmar, formerly Burma. Contributions to Mineralogy and Petrology, 145, 355–376.
Sorensen, S.S. and Harlow, G.E (1998) A cathodoluminescence (CL)-guided ion and electron microprobe tour of jadeitite chemistry and petrogenesis. Geological Society of America Abstracts with Programs, 30, A-60.
Spandler, C., Hermann, J., Arculus, R., and Mavrogenes, J. (2003) Redistribution of trace elements during prograde metamorphism from lawsonite blueschist to eclogite facies; implications for deep subduction-zone processes. Contributions to Mineralogy and Petrology, 146, 205–222.
Stalder, R., Foley, S.F., Brey, G.P., and Horn, I. (1988) Mineral-aqueous fluid partitioning of trace elements at 900–1200 °C and 3.0 to 5.7 GPa: new experimental data for garnet, clinopyroxene, and rutile and implications for mantle metasomatism. Geochimica et Cosmochimica Acta, 62, 1781–1801.
Tatsumi, Y. and Eggins S. (1995) Subduction Zone Magmatism, 225 p. Blackwell, Oxford.
Taylor, H.P., Jr. (1968) The oxygen isotope geochemistry of igneous rocks. Contributions to Mineralogy and Petrology, 19, 1–71.
Valley, J.W., Kitchen, N., Kohn, M.J., Niendorf, C.R., and Spicizza, M.J. (1995) UWG-2, a garnet standard for oxygen isotope ratios: Strategies for high precision and accuracy with laser heating. Geochimica et Cosmochimica Acta, 59, 5523–5531.
Washington H.S. (1906), in Bishop, H.R., commissioner, The Bishop Collection - Investigations and Studies in Jade. 2 volumes. New York, The DeVinne Press.
Yoder, H.S., Jr. (1950) The jadeite problem; parts I and II. American Journal of Science, 248, 225–248 and 312–334.
Yoder, H.S. and Chesterman, C.W. (1951) Jadeite of San Benito County, California. California Division of Mines and Geology Special Report 10-C.
Zack, T., Tomascak, P.B., Rudnick, R.L., Dalpe, C., and McDonough, W.F. (2003) Extremely light Li in orogenic eclogites: The role of isotope fractionation during dehydration in subducted oceanic crust. Earth and Planetary Science Letters, 208, 279–290.
Zheng, Y.-F. (1993) Calculation of oxygen isotope fractionation in anhydrous silicate minerals. Geochimica et Cosmochimica Acta, 57, 1079–1091.

MANUSCRIPT RECEIVED MARCH 23, 2005
MANUSCRIPT ACCEPTED FEBRUARY 3, 2006
MANUSCRIPT HANDLED BY WILLIAM CARLSON